Image Cover Sheet

CLASSIFICATION	SYSTEM NUMBER
UNCLASSIFIED	499676

TITLE

ANALYSIS OF THE CALIBRATION DATA MEASURED WITH A HIGH-FREQUENCY ANTENNA ARRAY

System Number:

Patron Number:

Requester:

Notes:

DSIS Use only:

Deliver to:

National Defence / Défense nationale

ANALYSIS OF THE CALIBRATION DATA MEASURED WITH A HIGH-FREQUENCY ANTENNA ARRAY (U)

by

Xinping Huang and Eric K.L. Hung

DEFENCE RESEARCH ESTABLISHMENT OTTAWA
REPORT NO. 1289

Canada

August 1996
Ottawa

National Defence
Défense nationale

ANALYSIS OF THE CALIBRATION DATA MEASURED WITH A HIGH-FREQUENCY ANTENNA ARRAY (U)

by

Xinping Huang
Applied Silicon Inc. Canada

and

Eric K.L. Hung
Surface Radar Section

DEFENCE RESEARCH ESTABLISHMENT OTTAWA
REPORT NO. 1289

PCN
05B09

August 1996
Ottawa

ABSTRACT

This report contains an analysis of the antenna calibration data taken with a high frequency (HF) antenna array and a pilot source towed behind a small aircraft. The analysis used an array calibration method developed by E.K.L. Hung. The objective was to determine whether this method was adequate for calibrating the HF antenna arrays in the Canadian Forces Supplementary Radio (CFSRS) modernization project.

The study showed that the calibration method significantly improved the performance of the array in detecting low-elevation (11° or less) targets and estimating their directions. The degree of improvement decreased as the target elevation increased. At an elevation of 49°, it was marginal at best.

This study also uncovered the presence of systematic errors in the calibration data. These errors increased rapidly with the pilot source elevation.

It is not possible to decide whether or not the calibration method is adequate for the CFSRS antenna arrays. In this study, the calibration method could be inadequate for high-elevation targets, or the method was adequate but the systematic errors negated the improvements gained in the calibration.

RÉSUMÉ

Ce rapport présente une analyse des données de calibration recueillies avec un réseau d'antennes décamétriques et une source témoin remorquée derrière un petit avion. L'analyse utilise une méthode de calibration d'antennes développée par E. K. L. Hung. L'objectif de cette analyse est de déterminer si cette méthode est adéquate pour la calibration d'antennes décamétriques utilisées dans le projet de modernisation du réseau radio supplémentaire des Forces canadiennes (RRSFC).

L'étude démontre que la méthode de calibration améliore considérablement la performance de l'antenne lors de la détection de cibles à petit angle de site (11° ou moins) et lors de l'estimation de leurs directions. Le facteur d'amélioration décroît lorsque l'angle de site de la cible augmente. À un angle de site de 49°, l'amélioration est tout au plus marginale.

Cette étude a aussi permis de découvrir la présence d'erreurs systématiques dans les données de calibration. Ces erreurs augmentent rapidement avec l'angle de site de la source témoin.

Il n'est pas possible de déterminer si la méthode suggérée est adéquate pour le réseau d'antennes décamétriques utilisé dans le projet de modernisation du RRSFC. Dans cette étude, la méthode de calibration est soit inadéquate pour de grands angles de site ou elle est adéquate mais les erreurs systématiques annulent les améliorations obtenues dans la calibration.

EXECUTIVE SUMMARY

This report contains an analysis of the calibration data taken with a high frequency (HF) antenna array in 1994 at Leitrim, near the Ottawa airport. It uses an array calibration method developed by Eric K.L. Hung. The objective is to determine whether this method is adequate for calibrating the HF antenna arrays in the Canadian Forces Supplementary Radio Systems (CFSRS) modernization project. These arrays are used for detecting long-range HF signals and estimating their directions.

Calibration optimizes the performance of antenna arrays in target detection and direction finding.

The method developed by Hung is unique. It is highly tolerant to the presence of interfering signals, including unknown specular multipath signals. Other calibration methods do not have this property. They cannot be used to calibrate the CFSRS arrays, because interfering signals are always present in HF antenna environments.

The following observations are based on the analysis of data files generated with transmitter ranges not less than 7 km and transmitter elevations not higher than 11°.

1. With a few exceptions, the calibration method increases the signal-to-interference-plus-noise ratio (SINR) in the array snapshots by a factor of 2 to 4 (3 to 6 dB). Because of this general increase, the method helps us detect signals that are undetectable before calibration. It also reduces the integration time needed to raise the SINRs of the desired signals to the minimum detectable level.

2. The calibration method increases the accuracy of target

direction estimates. More specifically, it reduces the standard deviation of the errors in bearing estimates by a factor of 3.0 or more.

3. The method increases the resolution performance of the antenna array. On the average, it reduces the number of array snapshots with unresolvable equal-strength signals by a factor of 2 or more.

Other data files, generated with shorter transmitter ranges and higher transmitter elevations, were available for the analysis. They required corrections for the perturbations in element response patterns as well as for the difference in transmitter elevations at the array elements. These corrections could not be carried out. Consequently, the authors hesitate to draw conclusions on the results they produced, although these results generally agreed with the above observations.

It is not yet possible to decide whether the calibration method developed by Hung is adequate for the HF antenna arrays in the CFSRS modernization project. The decision requires the analysis of calibration data generated with transmitter elevations higher than 11° and transmitter ranges not shorter than 7 km. These data are currently not available.

The difficulties in using the higher elevation files prompted the authors to study an alternative calibration method that tolerates the dependence of calibration coefficients on directions. Preliminary results indicated that this alternative method was superior to the method in this report. Because of these results, the authors have decided to stop further work on the method in this report and direct the remaining efforts to the evaluation of the alternative method.

TABLE OF CONTENTS

LIST OF FIGURES

LIST OF TABLES

1.0 INTRODUCTION

An accurate calibration of an antenna array is essential, if the array is to be used in direction-finding with high-resolution (HR) methods such as the MUSIC method [1]. Otherwise, the performance of these HR methods in estimating and resolving signal directions will be degraded.

Many methods to calibrate a narrowband antenna array have been published in the open literature. They include those by Paulraj and Kailath [2], Friedlander and Weiss [3,4], Brown, McClellan and Holder [5,6], and Pierre and Kaveh [7]. However, these methods cannot be used in array environments where unknown interfering signals, including diffuse and specular multipath signals, are present. In particular, they cannot be used to calibrate high-frequency (HF) antenna arrays, because multipath interfering signals are always present.

A unique calibration method [8] has recently been developed for HF antenna arrays at the Defence Research Establishment Ottawa (DREO). The method equalizes the gains and phases of the elements in antenna arrays. Unlike the methods in [2] to [7], it is highly tolerant to the presence of interfering signals, including unknown diffuse and specular multipath signals. In preliminary studies, this method produced highly accurate estimates of the element gains and phases.

This report contains an analysis of the calibration data measured in 1994 with an HF antenna array at Leitrim, near the Ottawa airport. It uses the calibration method in [8]. The main objective is to determine whether the method is adequate for calibrating the HF antenna arrays in the Canadian Forces Supplementary Radio Systems (CFSRS) modernization project.

The remainder of this report is organized as follows: Chapter 2 contains a description of the antenna array and the coordinate systems used in the analysis. Chapter 3 describes the calibration measurements and the data collected. Chapter 4 discusses the preprocessing of these calibration data. It includes checking the possible presence of faulty elements, Doppler filtering, and correcting the deviation of signal wavefronts from spherical wavefronts. The calibration method is presented in Chapter 5, and the estimates of element gains and phases obtained with this method are in Chapter 6. Chapter 7 provides an evaluation of the calibration method; it examines the effect of calibration on the accuracy of direction estimates, the signal-to-interference-plus-noise ratio (SINR) in the array snapshots, and the resolution of signal directions. The conclusions are given in Chapter 8.

2.0 ANTENNA ARRAY

The antenna array was located at Leitrim, which is near the Ottawa International Airport. It was planar, had twelve elements, and was part of a larger array with 52 elements. Each one of these elements was a six-meter high vertical monopole, implemented by a metal pipe standing on eight ground radials and fed approximately one-third of the way up. The positions of these elements are given in Table 1 and are plotted in Figure 1.

There are two coordinate systems in Table 1: a UVW-rectangular system supplied with the data and a polar system to be used in the analysis of calibration data. These systems are defined in Figure 2. In the rectangular system, the U-direction is the north direction, the V-direction is west, and the W-direction is up. In the polar system, the location of a point is identified by a triplet (r,θ,ψ). Here, r is the distance of the point from the origin, θ is the bearing angle, and ψ is the elevation angle. The bearing θ is measured in the UV-plane and clockwise from the U-axis.

The rectangular coordinates (u,v,w) and polar coordinates (r,θ,ψ) of a point in space are related to each other by:

$$u = r \cos\psi \cos\theta \ , \tag{2.1}$$

$$v = - r \cos\psi \sin\theta \ , \tag{2.2}$$

$$w = r \sin\psi \ , \tag{2.3}$$

and

$$r = (u^2+v^2+w^2)^{1/2} \ , \tag{2.4}$$

$$\theta = \tan^{-1}(-v/u) \ , \tag{2.5}$$

$$\psi = \tan^{-1}(w/(u^2+v^2)^{1/2}) \ . \tag{2.6}$$

The bearing θ is related to the azimuth angle θ_{az} in an XYZ-

coordinate system, defined with {X,Y,Z}={East,North,Up}, by

$$\theta_{az} = 90° - \theta \ . \tag{2.7}$$

The coordinates in the UVW and XYZ systems are related by

$$x = -v \ , \tag{2.8}$$
$$y = u \ , \tag{2.9}$$
$$z = w \ . \tag{2.10}$$

N	ELEMENT POSITIONS					
	Rectangle Coordinate			Polar Coordinate		
	u	v	w	r	θ	ψ
1	3.263	-24.786	0.0	25	82.5	0.0
2	-3.263	-24.786	0.0	25	97.5	0.0
3	-15.219	-19.834	0.0	25	127.5	0.0
4	-19.834	-15.219	0.0	25	142.5	0.0
5	-24.786	3.263	0.0	25	187.5	0.0
6	-19.834	15.219	0.0	25	217.5	0.0
7	23.097	9.567	0.0	25	337.5	0.0
8	24.786	3.263	0.0	25	352.5	0.0
9	85.001	22.776	0.0	88	345.0	0.0
10	-22.776	85.001	0.0	88	255.0	0.0
11	120.741	32.352	0.0	125	345.0	0.0
12	-32.352	120.741	0.0	125	255.0	0.0

Table 1. Element positions in the HF antenna array. Distances u, v, w, and r are measured in meters. Angles θ and ψ are measured in degrees.

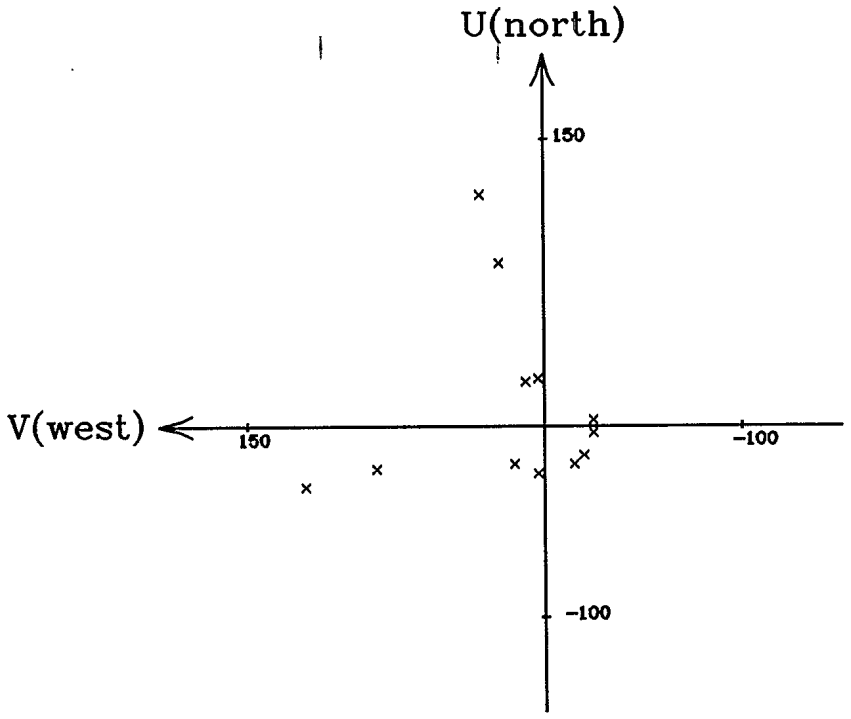

Figure 1. Geometry of Leitrim HF antenna array.

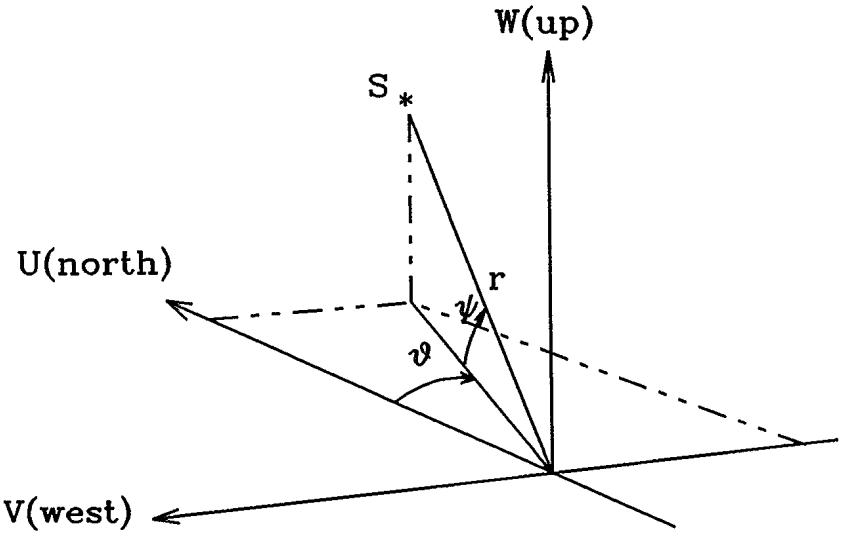

Figure 2. The UVW-rectangular coordinate system and the polar coordinate system.

3.0 CALIBRATION MEASUREMENTS

In the calibration measurements, a vertically oriented dipole transmitter was towed behind an airplane. This plane was flown along specified paths while snapshots of the outputs of the array elements were taken. Two global positioning systems were used to determine the ranges and directions of the transmitter in the snapshots. The first, identified as GPS1, was at the antenna site. Its output time, denoted by t1, was recorded with the array snapshots. The second, identified as GPS2, was a differential system consisting of two GPS receivers, one on the plane and the other on a known ground location. Its output time t2 and position $\mathbf{r}_{GPS2}(t2)$ were recorded in a log file on the aircraft at approximately one second intervals.

Six transmitter frequencies were used: 5.1, 7.5, 9.3, 11.5, 15.1, and 18.0 MHz. The outputs at each array element were downshifted in frequency to near-baseband and sampled with an A/D converter at 10.4 kHz. Approximately fifty data files were generated. Table 2 contains the nominal flight parameters and sizes for the files generated at 5.1 MHz. Each data block has 8000 array snapshots. Figures 3 to 10 illustrate the paths of the airplane in these files. They include five clockwise (CW) circles round the array, one counter-clockwise (CCW) circle round the array, and two straight lines over the array.

The flight path in File 2 has a side loop near bearing 210° and a hook near bearing 333°. Their presence are not in the flight plan. In later discussions, we shall refer to File 2 as the modified file with the side loop and the hook removed.

The transmitter was towed behind the airplane. Its location at the recorded GPS2 time t2 was approximately the same as that of

GPS2 at time t2-Δ, where Δ was equal to the GPS2-to-transmitter distance divided by the speed of the airplane. The value of Δ was approximately 2 seconds; its exact value depended on the wind speed, wind direction, plane speed, and plane direction at time t2.

In a separate study of the calibration data by Dr. R.W Jenkins [9], it was noted that the recorded GPS1 time t1 was not equal to the GPS2 time t2, recorded at the same time. These times were related by

$$t2 = t1-\epsilon \ , \tag{3.1}$$

where ϵ was a non-zero difference independent of frequency and transmitter elevation. The origin of this difference was unknown. This study also showed that the transmitter position at time t1, denoted by $\mathbf{r}_{TX}(t1)$, could be derived from the GPS2 position at t2 as

$$\begin{aligned} \mathbf{r}_{TX}(t1) &= \mathbf{r}_{GPS2}(t2-\Delta) \\ &= \mathbf{r}_{GPS2}(t1-\Delta') \ , \end{aligned} \tag{3.2}$$

where $\Delta'=\epsilon+\Delta$. The assignment

$$\Delta' = 8.7 \text{ seconds} \tag{3.3}$$

produced the best overall agreement between the estimated and measured transmitter directions.

File	Date	Planned Track				No. of Blocks
		Elevation (deg)	Altitude (ft)	Radius (km)	Direction	
1	18/05/94	4.5	3000	10	CW	2255
2	20/05/94	11	5000	7	CW	2308
3	20/05/94	11	5000	7	CCW	1438
4	24/05/94	18	6000	5	CW	1106
5	24/05/94	31	6150	3	CW	723
6	24/05/94	49	6000	2	CW	367
7	24/05/94		6000			1350
8	24/05/94		6000			1365

Table 2. Nominal flight parameters for the data files measured at 5.1 MHz. The date format is day/month/year. Each data block contains 8000 array snapshots

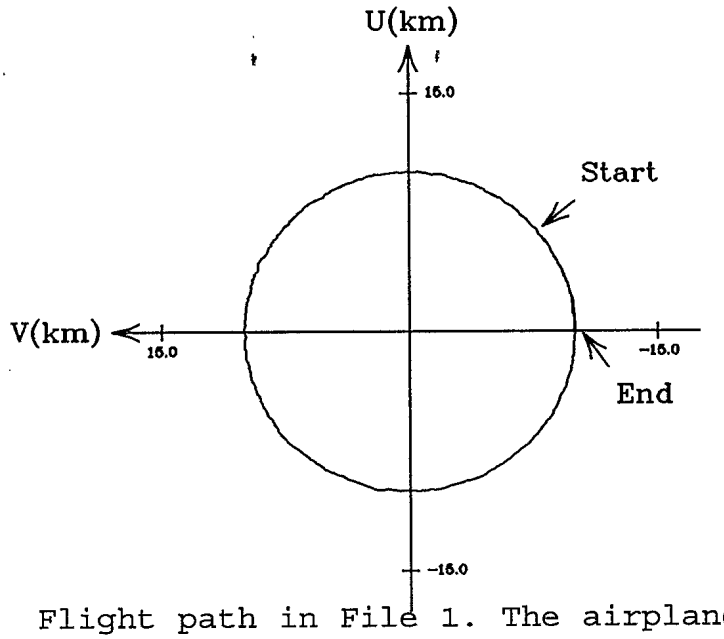

Figure 3. Flight path in File 1. The airplane circles the array with a radius of 10 km and proceeds clockwise (CW) through 405°, from north 45° east to north 90° east.

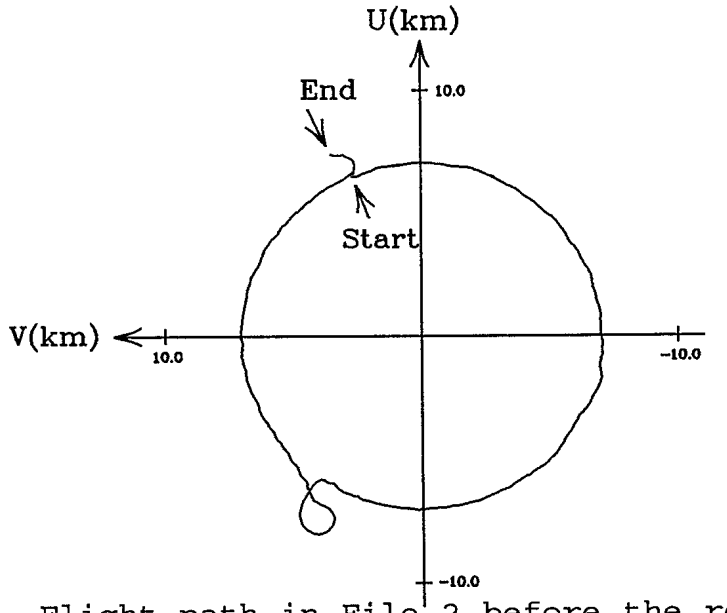

Figure 4. Flight path in File 2 before the removal of the side loop at bearing 210° and hook at bearing at 333°. The airplane circles the array with a radius 7 km, proceeds CW through 358°, from north 24° west to north 26° west.

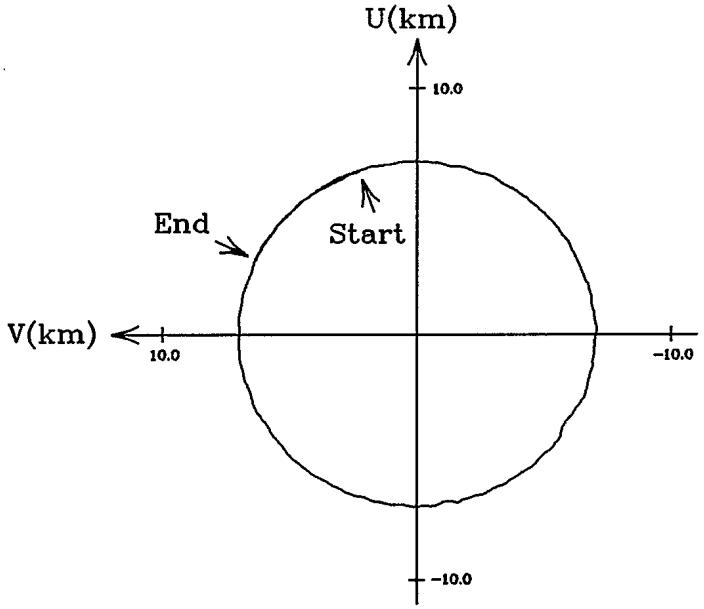

Figure 5. Flight path in File 3: range 7 km; counter-CW (CCW) 405°, north 19° west to north 64° west.

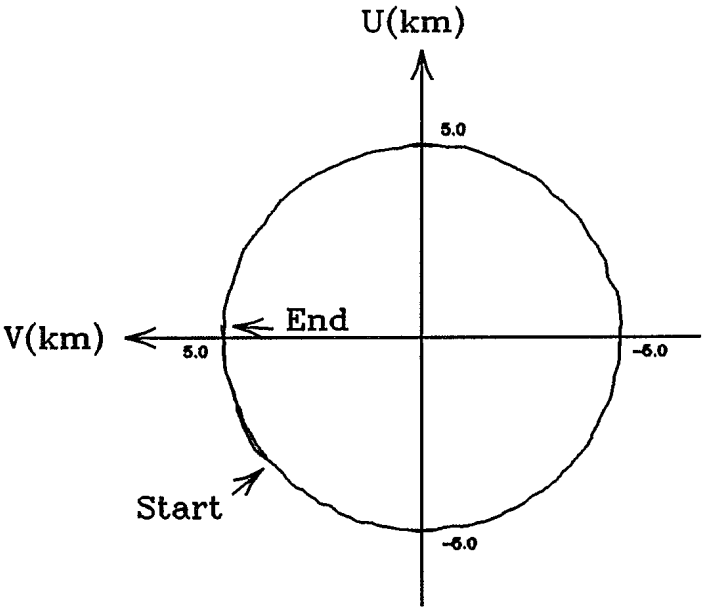

Figure 6. Flight path in File 4: range 5 km; CW 404°, south 49° west to north 57° west.

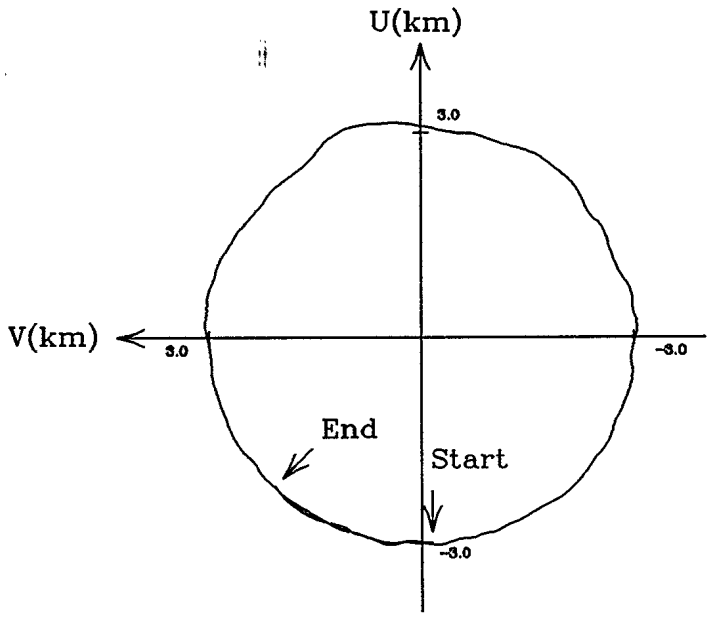

Figure 7. Flight path in File 5: range 3 km; CW 406°, south 3° east to south 43° west.

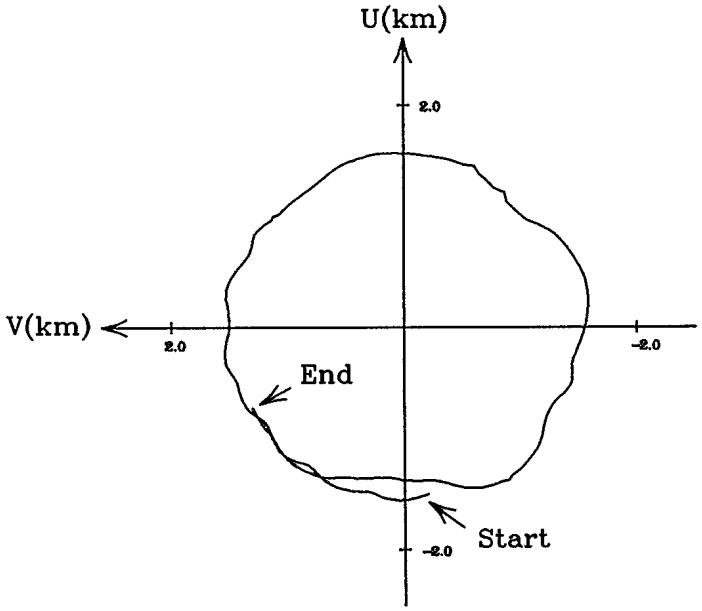

Figure 8. Flight path in File 6: range 1.5 km; CW 429°, south 8° east to south 61° west.

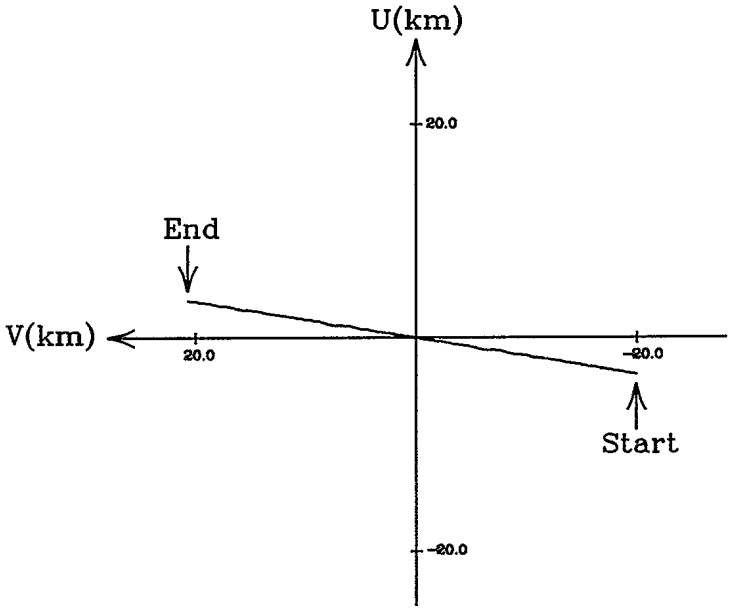

Figure 9. Flight path in File 7. It is a straight line over the array with a heading of west 9.7° north.

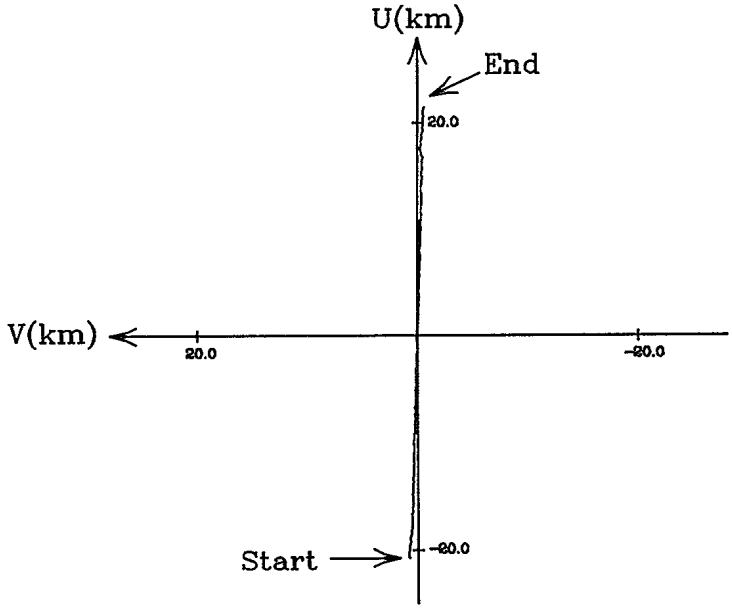

Figure 10. Flight path in File 8. It is a straight line over the array with a heading of north 1.0° east.

4.0 DATA PREPROCESSING

The data files were preprocessed before they were used to calculate the element gains and phases. The following is a list of the tasks in this preprocessing:

1. Check if there are faulty elements in the generation of the data files;

2. Reduce the number of array snapshots in each file by Doppler filtering; and

3. Correct the deviations of signal wavefronts from planar wavefronts in the filtered snapshots.

Task 2 is required, because the files are extremely large and have 2.9 to 19 million array snapshots per file.

Three corrections are ignored in the preprocessing. The first is the correction for the difference in the orientations of the array elements. It has been assumed that the metallic pipes used in the array elements were vertical and, therefore, parallel. The relative orientations of some pipes were checked, using the parallax method, in the summer of 1995. They were not exactly parallel, although the largest angle between any two pipes was at most a few degrees. This correction is ignored, because the orientations of the elements were not measured in the calibration experiments. The second correction is for the direction-dependent differences in the gain and phase response patterns of the array elements. These patterns were not identical in their direction dependence for the calibration measurements, although all were approximately dipole. This correction is ignored, because it depends on many unknown factors such as the ground conductivity,

vegetation, local structures, etc. The third correction is for the difference in the transmitter elevations at the array elements. The transmitter range was 10 km or less in the calibration experiment. Consequently, its elevation at each of the array elements was different in any particular array snapshot. This correction cannot be carried out, because it involves the unknown element patterns and orientations.

Ignoring the first two corrections produces perturbations in the gain and phase response patterns of the array elements. Usually, these perturbations are larger if the transmitter elevation is higher. Ignoring the last correction produces amplitude and phase errors at the outputs of the array elements. These errors are larger if the transmitter range is shorter.

File 6 in Table 2 was measured with nominal transmitter range and elevation of 2 km and 49°, respectively. Because the range was short and the elevation was high, we do not expect to get reliable results from this file. A large percentage of the array snapshots in Files 7 and 8 was measured with ranges shorter than 2 km and elevations higher than 49°. Consequently, we omit these files in later studies.

4.1 Faulty Element Check

The calibration measurements were such that, after Doppler filtering with a few hundred array snapshots or more, the transmitter signal at the array elements was very strong compared with all other signals. Therefore, the power spectrum calculated with the outputs of each array element should have a strong amplitude at the Doppler shifted frequency of the transmitter signal. It follows from this property that the array did not have faulty elements if (a) the spectrum of each element had a very strong signal present and (b) the frequency of this signal was the same at all elements.

Some results obtained in a check for faulty elements are presented in Figure 11. The input data used in Doppler filtering are the first 1000 array snapshots in Block #1 of the first 5.1 MHz data file. There are twelve spectra, one spectrum from the outputs of each array element. The strongest amplitude in each spectrum is at a baseband frequency of 1.95 kHz and is at least 25 dB stronger than the other signals. Therefore, the array did not have faulty elements during the generation of this 5.1 MHz file.

Only 1000 array snapshots are used to calculate each Doppler spectrum, although each data block has 8000 snapshots. The choice on the number of snapshots was influenced by many factors, e.g., the FFT frequency bin width must not be smaller than the bandwidth of the transmitter signal, the transmitter was swinging in the air, the transmitter antenna orientation was changing all the time, etc.

In the calculation of each spectrum, we augment the 1000 real output amplitudes of an element with 1048 zeros, convert the augmented sequence to a 2048 point complex frequency spectrum with the Fast Fourier Transform (FFT), and plot the powers of the positive frequency points only. The augmentation with zeros is necessary. Otherwise, the picket fence effect and noise presence could combine to prevent the strongest amplitude from appearing at the same frequency bin in all twelve spectra.

The FFT frequency bins are identified with one to 2048. Because the sampling frequency is 10.4 kHz, the frequency bandwidth of the bins is 10.4 Hz (= 10.4 kHz divided by 1000, the number of snapshots used in Doppler filtering) and the separation of the bins is 5.0781 Hz (= 10.4 kHz divided by 2048, the number of FFT bins). Bins 1025 to 2048 are negative frequency bins, because the array snapshots have in-phase (real) components only.

The above 1.95 kHz peak frequency is equal to $|f_s - f_o|$, where f_s is the frequency of the Doppler shifted transmitter signal at

the array elements and f_o is the frequency of the local oscillator in down conversion. It corresponds to the FFT frequency bin number 385, where the strongest amplitude is present.

There are three easily identifiable interfering signals in each spectrum. Their frequencies are 0, 0.06, and 3.08 kHz and their strengths are more than 25 below that of the strongest signal at 1.95 kHz. The 0 Hz interfering signal probably comes from an offset in the A/D converters. The origins of the others are not known.

The above three interfering signals are also present in all other 5.1 MHz files. An example is given in Figure 12, which is calculated with the first 1000 snapshots in Block #1 of the second 5.1 MHz file.

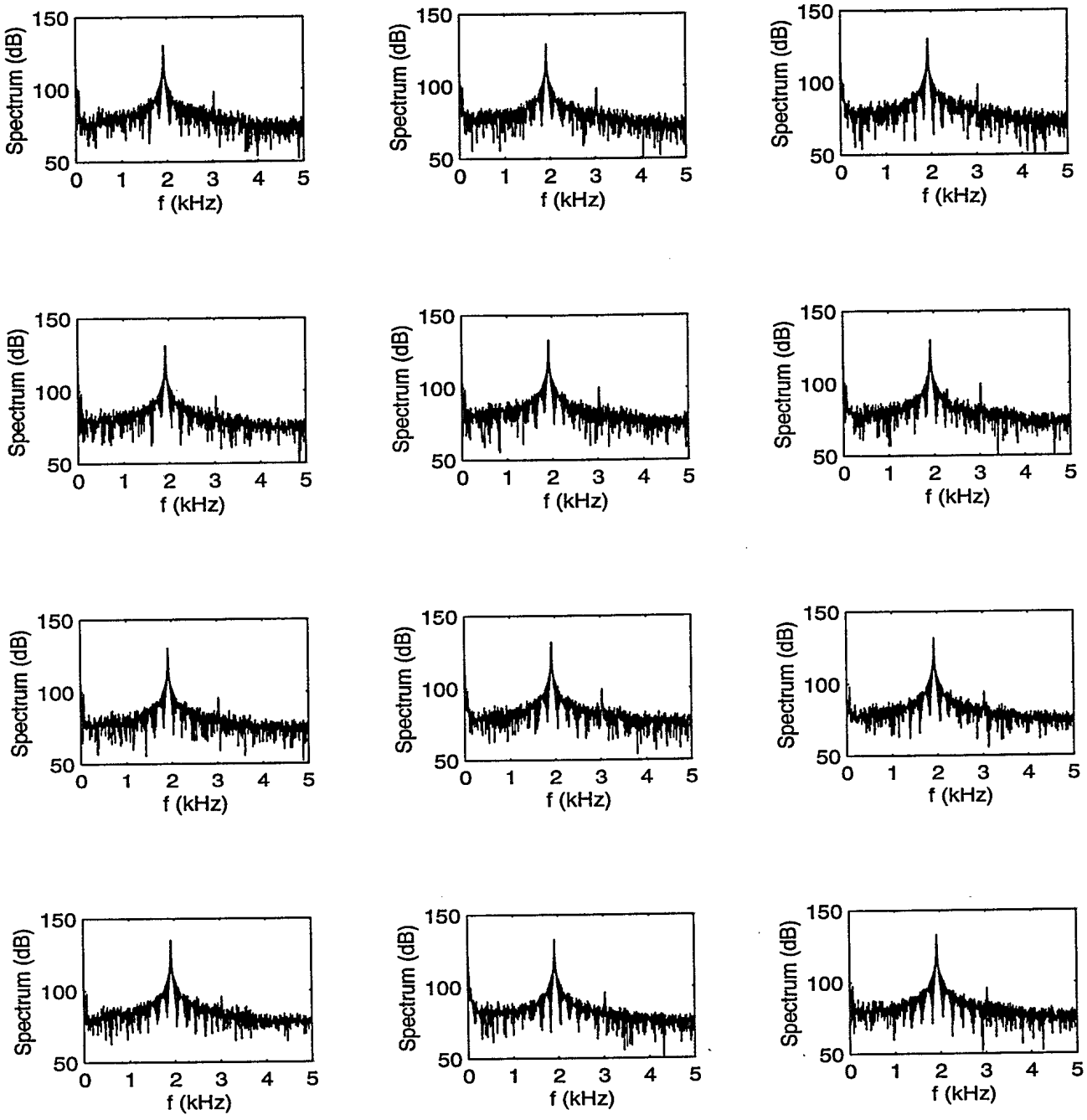

Figure 11. The spectra for each of the twelve array elements, using the first 1000 array snapshots in Block 1 of File 1.

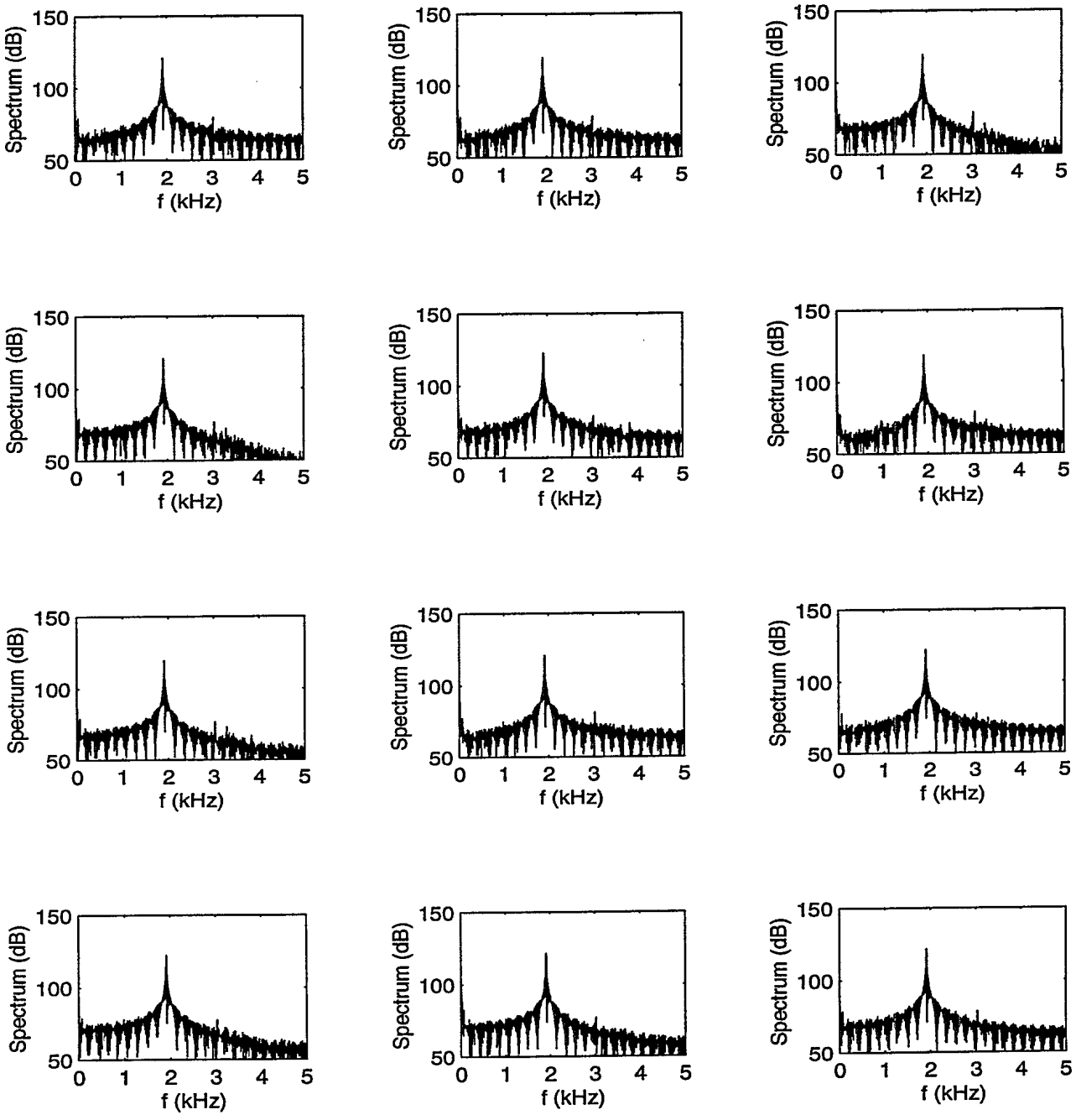

Figure 12. The spectra for each of the twelve array elements, using the first 1000 array snapshots in Block 1 of File 2.

4.2 Data Reduction

We use Doppler filtering to reduce the size of each data file by a factor 1000. The procedure described below takes note that the files are stored in blocks of 8000 array snapshots. There are two steps.

Step 1.

Separate each data block into eight sets with 1000 consecutive snapshots per set.

Step 2.

For each set,

(a) Augment the 1000 output amplitudes of each element with 1048 zeros;

(b) Calculate the 2048 point complex FFT frequency spectra of these augmented sequences;

(c) Study the spectrum calculated with the outputs of the first element. Identify the signal bin as the bin with the largest power. Ignore negative-frequency bins 1025 to 2048; and

(d) Construct a new array snapshot as

$$\tilde{\mathbf{x}} \triangleq (\tilde{x}_1, \tilde{x}_2, \tilde{x}_3, \cdots, \tilde{x}_{12})^T \ . \qquad (4.1)$$

In (4.1), $\tilde{x}_1$ to $\tilde{x}_{12}$ are the complex FFT amplitudes in the largest-signal bin of the spectra calculated from the outputs of elements 1 to 12, respectively. The superscript 'T' denotes the transpose.

The above procedure preserves the relative amplitudes of the transmitter signal at the array elements. It also maximizes the signal-to-noise ratio (SNR) in the array snapshots. Here, the ratio refers to the noise power in one FFT bin, which has a bandwidth of 10.4 Hz.

In later discussions, the transmitter location for $\tilde{\mathbf{x}}$ will be denoted by $\{r_t, \theta_t, \psi_t\}$ and will be defined as the average of the locations in the 1000 array snapshots used to construct $\tilde{\mathbf{x}}$.

4.3 Correction for Non-Planar Wavefront

The signal wavefront in $\tilde{\mathbf{x}}$ is not planar. We correct the deviation from a planar wavefront by replacing it with a new snapshot $\mathbf{x}$ with components $\{x_1, x_2, \cdots, x_{12}\}$ given by

$$x_n = (s_n/r_t) \{\exp[j2\pi(s_n - r_t)/\lambda] \; a_n(\theta_t, \psi_t)\} \; \tilde{x}_n \qquad n=1,2,\cdots,12. \tag{4.2}$$

In this expression,

$\{s_1, s_2, s_3, \cdots, s_{12}\}$ = element distances from transmitter,

λ = signal wavelength (= 58.82 m at 5.1 MHz) ,

and

$$a_n(\theta_t, \psi_t) = \exp[j2\pi(u_n \cos\psi_t \cos\theta_t - v_n \cos\psi_t \sin\theta_t + w_n \sin\psi_t)/\lambda] \; . \tag{4.3}$$

The first term, (s_n/r_t), in (4.2) corrects the r^{-2} dependence of signal power on range; the second term, $\{\cdots\}$, equalizes the signal phases at the elements; and $a_n(\theta_t, \psi_t)$ is the nth component of the array steering vector for direction $\{\theta_t, \psi_t\}$ and infinite range.

5.0 CALIBRATION METHOD

A brief description of the array calibration method in [8] is presented here. It contains the assumptions made, the signal model used, the theory for estimating the element gains and phases, and the procedure.

In the presentation, the set of element gains are denoted by the vector $\mathbf{g}$ or, equivalently, the set $\{g_n: n=1,2,\cdots,12\}$. Similarly, the set of element phases are denoted by $\boldsymbol{\phi}$ or $\{\phi_n: n=1,2,\cdots,12\}$. For convenience, the following uniqueness conditions are imposed on the gains and phases:

$$g_1 = 1 \ , \tag{5.1}$$

$$\phi_1 = 0 \ . \tag{5.2}$$

5.1 Assumptions

The following assumptions have been made in the development of the calibration method in [8]:

1. The relative gain responses of the array elements are independent of elevation and azimuth,

2. The relative phase responses of the array elements are independent of direction,

3. The mutual coupling among the elements can be ignored,

4. The signal-to-interference-plus-noise ratios (SINRs) at the array elements are reasonably high,

5. The calibration signal is effectively uncorrelated with the interfering signals in the data, and

6. The average signal-plus-noise powers incident upon the array elements are the same.

The relative gain and phase responses are also known as the element gains and phases, respectively.

We do not examine the validity of the assumptions in this report. We only study what one can gain when the method in [8] is used to calibrate the antenna array at Leitrim.

5.2 Signal Model

In this signal model, a preprocessed array snapshot has the decomposition

$$\mathbf{x} = \alpha\, \mathbf{b}(\mathbf{g},\boldsymbol{\phi},\theta_t,\psi_t) + \text{interference} + \text{noise}. \tag{5.3}$$

The first term represents the direct signal from the transmitter. Here, α is the complex signal amplitude at a reference element in the array and $\mathbf{b}(\mathbf{g},\boldsymbol{\phi},\theta_t,\psi_t)$ is the array manifold vector for the transmitter direction (θ_t,ψ_t).

The array manifold vector for any direction (θ,ψ) is given by

$$\mathbf{b}(\mathbf{g},\boldsymbol{\phi},\theta,\psi) = \mathbf{G}(\mathbf{g})\ \mathbf{T}(\boldsymbol{\phi})\ \mathbf{a}(\theta,\psi), \tag{5.4}$$

where $\mathbf{G}(\mathbf{g})$ and $\mathbf{T}(\boldsymbol{\phi})$ are N×N diagonal matrices associated with the element gains and phases, respectively, and, under the assumptions, are defined as

$$\mathbf{G}(\mathbf{g}) = \text{diag}\{g_1, g_2, \cdots, g_{12}\}, \tag{5.5}$$

and

$$\mathbf{T}(\boldsymbol{\phi}) = \mathrm{diag}\{\exp[j\phi_1], \exp[j\phi_2], \cdots, \exp[j\phi_{12}]\} \ . \qquad (5.6)$$

5.3 Theory

The theoretical development initially discusses the estimation of element gains. Next, it presents a transformation that equalizes the gains and simultaneously 'fixes' the transmitter direction in the data. Finally, it explains how one can estimate the element phase responses with the transformed data.

5.3.1 Estimation of Element Gains

The expected values of the incident signal-plus-noise powers are equal at the array elements. Consequently, the expected values of the output powers at these elements are proportional to the squares of the element gains. If these output powers are $\{p_1, p_2, \cdots, p_{12}\}$, the ratio p_n/g_n^2 is independent of the element identification n.

Given a set of estimates $\{\hat{p}_n: \ n=1,2,\cdots,12\}$, the gain estimates can be calculated as

$$\hat{g}_n = \sqrt{\frac{\hat{p}_n}{\hat{p}_1}} \ , \qquad n=1,2,\cdots,12, \qquad (5.7)$$

since condition (5.1) requires $\hat{g}_1=1$. One can show that an accurate estimation of the average output powers would result in an accurate estimation of the element gains.

5.3.2 Transformation for Snapshots

The array manifold vector for the transmitter direction is given by (5.4), with $\theta=\theta_t$ and $\psi=\psi_t$. Because $\mathbf{G}(\mathbf{g})$ and $\mathbf{T}(\boldsymbol{\phi})$ are both diagonal, a simple rearrangement leads to

$$\mathbf{b}(\mathbf{g},\boldsymbol{\phi},\theta_t,\psi_t) = \mathbf{G}(\mathbf{g})\ \mathbf{A}(\theta_t,\psi_t)\ \boldsymbol{\tau}(\boldsymbol{\phi}), \tag{5.8}$$

where

$$\mathbf{A}(\theta_t,\psi_t) = \mathrm{diag}\{a_1(\theta_t,\psi_t), a_2(\theta_t,\psi_t), \cdots, a_N(\theta_t,\psi_t)\}. \tag{5.9}$$

The set $\{a_n(\theta_t,\psi_t): n=1,2,\cdots,12\}$ represents the components of the array steering vector $\mathbf{a}(\theta_t,\psi_t)$. Vector $\boldsymbol{\tau}(\boldsymbol{\phi})$ is given by

$$\boldsymbol{\tau}(\boldsymbol{\phi}) = (\exp[j\phi_1], \exp[j\phi_2], \cdots, \exp[j\phi_{12}])^T \tag{5.10}$$

and is constructed with the element phases.

The rearranged expression (5.8) makes the array steering phases in $\mathbf{a}(\theta_t,\psi_t)$ behave like element phases. It also makes $\boldsymbol{\tau}(\boldsymbol{\phi})$ behave like an array steering vector.

Let a transformation matrix, dependent on the calibration source direction (θ_t,ψ_t), be defined as

$$\boldsymbol{\Gamma}(\mathbf{g},\theta_t,\psi_t) \triangleq \mathbf{A}^{-1}(\theta_t,\psi_t)\ \mathbf{G}^{-1}(\mathbf{g}). \tag{5.11}$$

This matrix has the property that

$$\boldsymbol{\Gamma}(\mathbf{g},\theta_t,\psi_t)\ \mathbf{b}(\mathbf{g},\boldsymbol{\phi},\theta,\psi) = \mathbf{A}^{-1}(\theta_t,\psi_t)\ \mathbf{A}(\theta,\psi)\ \boldsymbol{\tau}(\boldsymbol{\phi}). \tag{5.12}$$

The vector on the right-hand side has components with unit magnitudes. It can be interpreted as an array steering vector for a new and usually non-physical 'direction' associated with the transformation. For $(\theta,\psi)=(\theta_t,\psi_t)$, this vector becomes $\boldsymbol{\tau}(\boldsymbol{\phi})$ and is independent of (θ_t,ψ_t).

Applied to the calibration data, the transformation converts each array snapshot to a new one given by

$$\begin{aligned} \mathbf{y} &= \mathbf{\Gamma}(\mathbf{g}, \theta_t, \psi_t)\ \mathbf{x} \\ &= \mathbf{\Gamma}(\mathbf{g}, \theta_t, \psi_t)\ [\alpha\ \mathbf{b}(\mathbf{g}, \boldsymbol{\phi}, \theta_t, \psi_t) + \text{interference} + \text{noise}] \\ &= \alpha\ \mathbf{A}^{-1}(\theta_t, \psi_t)\ \mathbf{A}(\theta_t, \psi_t)\ \boldsymbol{\tau}(\boldsymbol{\phi}) + \mathbf{z} \\ &= \alpha\ \boldsymbol{\tau}(\boldsymbol{\phi}) + \mathbf{z} \end{aligned} \tag{5.13}$$

where $\mathbf{z}$ represents the contributions of the interference and noise. The first term is the transform of the direct signal from the transmitter. This signal has an amplitude α and a non-physical fixed 'direction' determined by $\boldsymbol{\tau}(\boldsymbol{\phi})$. The second term is not correlated with the first, because the direct signal is not correlated with the interfering signals in the original snapshots. Moreover, the direction of each interfering signal in this term depends on (θ_t, ψ_t) as well as the original direction of the interfering signal.

Because the first term on the right-hand-side of (5.13) has a fixed direction determined by $\boldsymbol{\tau}(\boldsymbol{\phi})$, one can used a direction finding method to estimate the element phases from the transformed array snapshots. A technique that allows the user to modify the individual phases in the array steering vectors must be used. The 'directional power spectrum' it produces is a function of the trial element phases.

5.3.3 Estimation of Element Phases

The Capon method [9] is used in direction-finding. From (5.13), the data covariance matrix in this calculation is

$$\begin{aligned} \mathbf{R}_y &= E\{\mathbf{y}\ \mathbf{y}^H\} \\ &= |\alpha|^2\ \boldsymbol{\tau}(\boldsymbol{\phi})\ \boldsymbol{\tau}^H(\boldsymbol{\phi}) + \mathbf{R}_z, \end{aligned} \tag{5.14}$$

where $E\{\cdot\}$ denotes the expected value, $|\alpha|^2=E\{|\alpha_m|^2\}$, and $\mathbf{R}_z=E\{\mathbf{z}\mathbf{z}^H\}$. The second line strongly indicates that a directional spectrum calculated with $\mathbf{R}_y$ would have a strong peak in the direction corresponding to $\tau(\phi)$. A more detailed analysis is given below.

Let $\tilde{\phi}$ be a trial value of ϕ in the calculation. The output power calculated with the Capon method is

$$\mathcal{P}(\tilde{\phi},\mathbf{R}_y) \triangleq \frac{1}{F(\tilde{\phi},\mathbf{R}_y,\tilde{\phi})} , \tag{5.15}$$

where

$$F(\phi_a,\mathbf{R}_y,\phi_b) = \tau^H(\phi_a)\ \mathbf{R}_y^{-1}\ \tau(\phi_b) . \tag{5.16}$$

Because $\mathbf{R}_y$ is given by (5.13), application of the matrix inversion lemma leads to

$$\mathbf{R}_y^{-1} = \mathbf{R}_z^{-1} - \frac{|\alpha|^2\ \mathbf{R}_z^{-1}\tau(\phi)\ \tau^H(\phi)\ \mathbf{R}_z^{-1}}{1 + |\alpha|^2\ F(\phi,\mathbf{R}_z,\phi)} , \tag{5.17}$$

and

$$\mathcal{P}(\tilde{\phi},\mathbf{R}_y) = \frac{1 + |\alpha|^2\ F(\phi,\mathbf{R}_z,\phi)}{F(\tilde{\phi},\mathbf{R}_z,\tilde{\phi}) + |\alpha|^2\ H(\phi,\mathbf{R}_z,\tilde{\phi})} , \tag{5.18}$$

with

$$\begin{aligned} H(\phi,\mathbf{R}_z,\tilde{\phi}) &= F(\phi,\mathbf{R}_z,\phi)\ F(\tilde{\phi},\mathbf{R}_z,\tilde{\phi}) - |F(\phi,\mathbf{R}_z,\tilde{\phi})|^2 \\ &= \|\mathbf{q}\|^2\ \|\tilde{\mathbf{q}}\|^2 - |\mathbf{q}^H\ \tilde{\mathbf{q}}|^2 . \end{aligned} \tag{5.19}$$

Here, $\|\cdot\|$ represents the Euclidean norm. The second line is obtained by noting that $\mathbf{R}_z^{-1}$ is the inverse of an N×N non-singular correlation matrix when noise is present and that it has the decomposition

$$\mathbf{R}_z^{-1} = \mathbf{V}^H \mathbf{V}, \tag{5.20}$$

where $\mathbf{V}$ is a non-singular NxN matrix also. This gives, for example,

$$\begin{aligned} F(\phi, \mathbf{R}_z, \tilde{\phi}) &= \tau^H(\phi)\ \mathbf{R}_z^{-1}\ \tau(\tilde{\phi}) \\ &= \tau^H(\phi)\ \mathbf{V}^H\ \mathbf{V}\ \tau(\tilde{\phi}) \\ &= \mathbf{q}^H\ \tilde{\mathbf{q}}\ , \end{aligned} \tag{5.21}$$

where

$$\mathbf{q} = \mathbf{V}\ \tau(\phi) \tag{5.22}$$

and

$$\tilde{\mathbf{q}} = \mathbf{V}\ \tau(\tilde{\phi})\ . \tag{5.23}$$

From (5.11) and the Schwartz's inequality

$$H(\phi, \mathbf{R}_z, \tilde{\phi}) \geq 0. \tag{5.24}$$

The equality sign holds if and only if $\tilde{\phi}=\phi$.

The above results indicate that one can obtain an estimate of ϕ by maximizing $\mathcal{P}(\tilde{\phi}, \mathbf{R}_y)$ with respect to $\tilde{\phi}$, provided that the rate at which $F(\tilde{\phi}, \mathbf{R}_z, \tilde{\phi})$ changes in the neighbourhood of ϕ is small compared with that of $|\alpha|^2 H(\phi, \mathbf{R}_z, \tilde{\phi})$. Increasing $|\alpha|$ yields a more accurate estimate of ϕ. Making $F(\tilde{\phi}, \mathbf{R}_z, \tilde{\phi})$ independent of $\tilde{\phi}$ leads to $\tilde{\phi}=\phi$ at the maximum.

5.4 Procedure

The procedure to calculate the element gains and phases has five steps. Step 5 involves the maximization of an objective

function, and the implementation of this step is discussed separately.

5.4.1 Steps in Procedure

Let $\{\mathbf{x}_m: m=1,2,\cdots,M\}$ be a set of M array snapshots. Let the corresponding transmitter directions be $\{(\theta_m,\psi_m): m=1,2,\cdots, M\}$. The procedure to estimate the element gains and phases is given below.

Step 1.

Calculate the estimates of the element gains with (5.7). Denote the results by $\{\hat{g}_n: n=1,2,\cdots,12\}$.

Step 2.

Transform the snapshots to a new set $\{\mathbf{y}_m: m=1,2,\cdots,M\}$ with

$$\mathbf{y}_m = \mathbf{\Gamma}(\hat{\mathbf{g}},\theta_m,\psi_m)\ \mathbf{x}_m\ , \qquad m=1,2,\cdots,M, \tag{5.25}$$

where $\mathbf{\Gamma}(\hat{\mathbf{g}},\theta_m,\psi_m)$ is given by (5.11), and $\hat{\mathbf{g}}$ denotes the set of gain estimates.

Step 3.

Calculate an estimate of the data covariance matrix as

$$\hat{\mathbf{R}}_y = \frac{1}{M}\sum_{m=1}^{M} \mathbf{y}_m\ \mathbf{y}_m^H \tag{5.26}$$

Step 4.

Define a function $\mathcal{P}(\tilde{\boldsymbol{\phi}},\hat{\mathbf{R}}_y)$ with (5.15) and (5.16), using $\hat{\mathbf{R}}_y$ instead of $\mathbf{R}_y$.

Step 5.

Identify the estimate $\hat{\phi}$ as the $\tilde{\phi}$ that maximizes $\mathcal{P}(\tilde{\phi},\hat{\mathbf{R}}_y)$.

5.4.2 Implementation of Step 5

Step 5 in the procedure requires the location of the global maximum of $\mathcal{P}(\tilde{\phi},\mathbf{R}_y)$. In a computer simulation to study the problems that may arise, the following results are observed:

1. The directional power $\mathcal{P}(\tilde{\phi},\mathbf{R}_y)$, as a function of $\tilde{\phi}$, is usually not unimodal. However, the global maximum is usually the one closest to the true ϕ.

2. The finite precision in computer arithmetic adds a small random error to the true value of $\mathcal{P}(\tilde{\phi},\mathbf{R}_y)$. This error is very difficult to handle in the search for the global maximum, unless the constraint (5.2) is imposed on every $\tilde{\phi}$ in the calculation of the function. The random error also generates many false maxima in the neighbourhood of each true maximum. The density and peak values of these false maxima generally increase as the Euclidean distance from the true maximum decreases or as the value of the true maximum increases.

Based on the above observations, the search for the global maximum is divided into two steps as follows:

Step 5A.

Initialize the components of $\tilde{\phi}$ as samples of a random variate uniformly distributed in the range [-90°,90°], assuming that the true element phases do not deviate from zero by more than 90°. Use hill-climbing with random searches at each local maximum. Modify the components of $\tilde{\phi}$ individually. Impose (5.2) on each modified $\tilde{\phi}$ before calculating the corresponding

$\mathcal{P}(\tilde{\phi}, \hat{R}_y)$.

Step 5B.

Repeat Step 5A K times, where K is a large number. Denote the maximum positions and power values by $\{(\hat{\phi}_k, \mathcal{P}_k) : k=1,2,\cdots,K\}$, respectively. Identify the largest $\mathcal{P}_k$ as the value at the global maximum and denote it by $\hat{\mathcal{P}}$. Identify the corresponding $\tilde{\phi}_k$ as the estimate $\hat{\phi}$.

6.0 GAIN AND PHASE ESTIMATES

A subset of approximately three thousand array snapshots is extracted from each preprocessed file produced in Chapter 4. The element gains and phases obtained from these subsets are then studied.

The procedure to construct a subset initially isolates a file section that spans 360° in bearing. Next, it generates a set of M dummy bearings as

$$\tilde{\theta}_m = \theta_1 + 360(m-1)/M \ . \qquad m=1,2,\cdots,M-1 \ , \qquad (6.1)$$

where θ_1 is the bearing of the first snapshot in this isolated section. Finally, it identifies the snapshot with bearing closest to $\tilde{\theta}_m$ as $\mathbf{x}_m$ and denotes the direction of this snapshot as $\{\theta_m, \psi_m\}$.

It has been stated in Chapter 4 that three corrections have been ignored in data preprocessing; ignoring the first two corrections produce perturbations in the gain and phase response patterns of the array elements; these perturbations are usually larger if the transmitter elevation is higher; ignoring the last correction produces amplitude and phase errors at the outputs of the array elements; and these errors are larger if the transmitter range is shorter. Consequently, the element gain and phase estimates obtained from any file are actually the average of the perturbed gains and phases in the file. Besides, the errors in estimating these average values are larger if the transmitter elevation is higher. In the discussion of results, we therefore give more credibility to the estimates calculated with Files 1, 2 and 3, where the nominal transmitter ranges in Table 2 are 10 km, 7 km and 7 km, respectively, and the corresponding transmitter elevations are 4.5°, 11° and 11°, respectively. We are also non-

committal in the remarks on the estimates calculated with File 6 where the nominal range and elevations are 2 km and 49°, respectively.

In Tables 3 and 4 are the element gain and phase estimates, respectively, obtained with Files 1 to 6. Table 5 contains the transmitter range, transmitter elevation, the values of M used to calculate the estimates, the average of the gain values in the set $\{\hat{g}_1, \hat{g}_2, \ldots, \hat{g}_{12}\}$, and the difference between the largest and the smallest values in this set. Some of the more important observations and remarks are given below.

1. The standard deviations of the errors in the gain estimates from File 2 and File 3 are approximately 0.004. Those of the phase estimates are approximately 0.2°.

   Remark: These standard deviations are derived from the differences in the estimates obtained from the two files. The differences come from the measurement errors in the estimates, because the transmitter ranges and elevations are the same in these files.

2. The elevation gain patterns of the elements are different.

   Remark: One evidence of this property comes from a direct comparison of the gain estimates in Table 3. Another evidence comes from Table 5, where ave$\{\hat{g}_n\}$ is the average of the gain values, diff$\{\hat{g}_n\}$ is the difference between the largest and the smallest gains, and diff/ave is the ratio diff$\{\hat{g}_n\}$/ave$\{\hat{g}_n\}$. The ratio diff/ave increases steadily from 0.190 for File 1 to 0.255 for File 6.

   Remark: This difference may indicate a real dependence of relative element gains on elevation.

3. The element phases are essentially the same in the first five files.

   Remark: This observation is based on a study of the phase estimates in Table 4. The largest and the smallest estimates in each row differ by 3.5° or less.

4. The phase estimates for elements n=10 to 12 are significantly different from those of the other elements.

n	Gain Estimate $\hat{g}_n$					
	File 1 (ψ=4.5°)	2 (11°)	3 (11°)	4 (18°)	5 (31°)	6 (49°)
1	1.0000	1.0000	1.0000	1.0000	1.0000	1.0000
2	0.9770	0.9948	0.9948	0.9757	0.9743	0.9852
3	1.0109	1.0184	1.0195	0.9949	1.0020	1.0295
4	1.0049	1.0122	1.0184	0.9969	1.0071	1.0348
5	1.1005	1.1330	1.1428	1.1069	1.1108	1.1477
6	1.0189	1.0501	1.0596	1.0201	1.0225	1.0665
7	0.9581	0.9938	1.0010	0.8970	0.9137	0.9198
8	1.0119	1.0481	1.0513	1.0262	1.0410	1.0496
9	0.9113	1.0706	1.0729	1.0988	1.1519	1.1867
10	0.9980	0.9836	0.9876	0.9828	0.9866	1.0169
11	0.9790	0.9979	0.9979	1.0292	1.0924	1.1350
12	0.9432	0.9365	0.9434	0.9223	0.9373	0.9926

Table 3. Gain estimates derived from the first six 5.1 MHz files. The target elevations are in brackets.

n	Phase Estimates $\hat{\psi}_n$ (deg)					
	File 1 (ψ=4.5°)	2 (11°)	3 (11°)	4 (18°)	5 (31°)	6 (49°)
1	0.0	0.0	0.0	0.0	0.0	0.0
2	0.8	0.5	0.6	0.2	-0.2	1.5
3	0.2	0.0	0.2	0.0	-0.4	2.3
4	-0.2	-0.2	-0.1	-0.4	-0.5	1.6
5	1.1	1.4	1.4	1.1	1.5	2.1
6	1.2	1.9	1.9	1.5	1.8	3.1
7	3.8	4.3	3.9	4.6	3.5	3.4
8	2.5	3.4	3.2	2.7	1.5	1.8
9	-0.1	1.1	0.8	0.4	-0.7	0.0
10	-7.9	-8.9	-9.4	-8.2	-6.6	-3.3
11	-30.2	-30.4	-30.1	-31.2	-32.4	-30.4
12	-12.1	-13.9	-14.3	-13.9	-10.8	-3.7

Table 4. Phase estimates derived from the first six 5.1 MHz files.

File	1	2	3	4	5	6
Range(km)	10	7	7	5	3	2
ψ(deg)	4.5	11	11	18	31	49
M	3600	3600	3600	3600	3600	2435
ave$\{\hat{g}_n\}$	0.993	1.020	1.024	1.004	1.020	1.047
diff$\{\hat{g}_n\}$	0.189	0.196	0.199	0.210	0.238	0.267
diff/ave	0.190	0.192	0.194	0.209	0.233	0.255

Table 5. Range, true target elevation ψ, number of snapshots used in estimation M, the average of the gain estimates in the set $\{\hat{g}_1, \hat{g}_2, \ldots, \hat{g}_{12}\}$, the difference between the largest and the smallest values in this set, and the difference divided by the average.

7.0 EVALUATION OF CALIBRATION METHOD

The gain and phase estimates obtained from File 2 are used to calibrate the preprocessed snapshots in Files 1 to 6. The effect of calibration on the performance of the antenna array is then studied. This study includes the accuracy of direction estimates, the signal-to-interference-plus-noise ratio (SINR) in the array snapshots, and the resolution of signal directions.

The file subsets constructed in Section 6 are used in this study. They have the convenient properties that each subset has neither too many nor too few snapshots; the transmitter circles the array once; and the snapshots are approximately equally spaced in bearing.

In the convention used, the calibrated snapshot derived from an uncalibrated snapshot $\mathbf{x}$ is denoted by $\mathbf{x}^c$. Its components are denoted by $\{x_1^c, x_2^c, \cdots, x_{12}^c\}$ and are calculated as

$$x_n^c = \hat{g}_n^{-1} \exp[-j\hat{\phi}_n]\ x_n\ , \qquad n=1,2,\cdots,12\ . \tag{7.1}$$

Here, $\{\hat{g}_1, \hat{g}_2, \cdots, \hat{g}_{12}\}$ and $\{\hat{\phi}_1, \hat{\phi}_2, \cdots, \hat{\phi}_{12}\}$ are the gain and phase estimates, respectively, obtained from File 2. Their values are given by Column 3 in Tables 3 and 4, respectively.

Although File 6 is included in the evaluation, we avoid making many comments on the results obtained with this file, because the transmitter range is too short and the transmitter elevation, too high.

7.1 Effect of Calibration on Direction Estimates

This study assumes that there is only one signal in each array

snapshot and that this signal is the direct signal from the transmitter. It uses the maximum likelihood method to estimate the bearing and elevation of this signal in the snapshots.

In the presentation of results, the error in a bearing estimate is defined as

$$\epsilon(\hat{\theta}) = \hat{\theta} - \theta \ , \qquad (7.2)$$

where $\hat{\theta}$ is the estimate and θ is the GPS bearing calculated with (3.2) and (3.3).

The errors in bearing estimates are plotted in point mode in Figures 13 to 18. Their mean and standard deviations are given in Table 6. Figures 19 to 24 contain the elevation estimates. Some notable observations are given below.

1. The estimates seem to fall on a smooth curve, although they are plotted in point mode.

   Remark: It appears that the SINR in the preprocessed snapshots is high and that the interfering environment does not change rapidly with bearing.

2. Before calibration, the errors in bearing estimates depend strongly on the bearing. In particular, the errors are above the average value near the 60° bearing and are below it near 240°. After calibration, only traces of this dependence remain.

3. The mean value of the bearing errors from each file is not zero. It is also file dependent.

   Remark: It appears the non-zero mean values originate from the assignment of Δ' in (3.3). One can make them equal to zero

by using the new values, denoted by Δ'(new), in Table 6.

Remark: The dependence of Δ'(new) on file number has no statistical significance. After calibration, for example, the difference between the largest and the smallest values of Δ'(new) is 0.7 second (= difference of values from Files 3 and 6). This difference corresponds to bearing errors of 0.06° for File 3 and 0.15° for File 6. These errors are small compared with the corresponding standard deviations in Column 5.

4. The gross features in Figures 14 and 15 are very similar, if the difference in mean values is ignored.

Remark: This property is consistent with the interpretation that the multipath interference in Files 2 and 3 is essentially the same and that the variations in bearing errors come mainly from the dependence of this interference on direction.

5. Before calibration, the standard deviation of the errors in bearing estimates are between 1.09° and 1.61°. After calibration, they are 0.85° or less.

Remark: The standard deviation after calibration appears to be highly correlated with the track deformations in Figures 3 to 8. This standard deviation is the smallest in the estimates from File 1, where the track is a near perfect circle. It is the largest from File 6, where the track is very much distorted.

6. The magnitudes of the elevation errors are generally smaller after calibration.

7. There are strings of near-zero elevation estimates in Figures 19 to 21.

Remark: Inadequate calibration may be a reason for this characteristic. One can verify by simulation that an increase in calibration error is usually accompanied by a reduction in the magnitudes of elevation estimates, since elevation errors have a proportional effect on the elevation cosine values rather than on the elevations themselves.

8. The errors in the elevation estimates depend on the true elevation. Usually, their magnitudes are larger if the true elevation is lower.

Remark: One reason for this property is the dependence of the array elevation beamwidth on elevation. This beamwidth is larger if the elevation is smaller.

9. There are more negative elevation errors than positive ones.

Remark: One reason is given in the remark in Observation 8.

10. The gross features in Figures 20 and 21 are very similar.

Remark: This property is consistent with Observation 4.

File	Mean$\{\epsilon(\hat{\theta})\}$ (deg)		Std$\{\epsilon(\hat{\theta})\}$ (deg)		Δ' (new) (second)	
	Uncal.	Cal.	Uncal.	Cal.	Uncal.	Cal.
1	-0.29	-0.30	1.09	0.32	7.4	7.4
2	-0.44	-0.43	1.19	0.40	7.4	7.4
3	0.61	0.62	1.16	0.39	7.0	6.9
4	-0.66	-0.65	1.23	0.38	7.3	7.3
5	-1.14	-1.13	1.29	0.39	7.2	7.2
6	-1.93	-1.67	1.61	0.85	7.4	7.6

Table 6. The means and standard deviations of the errors in bearing estimates, and the time adjustments needed to make the mean values equal to zero.

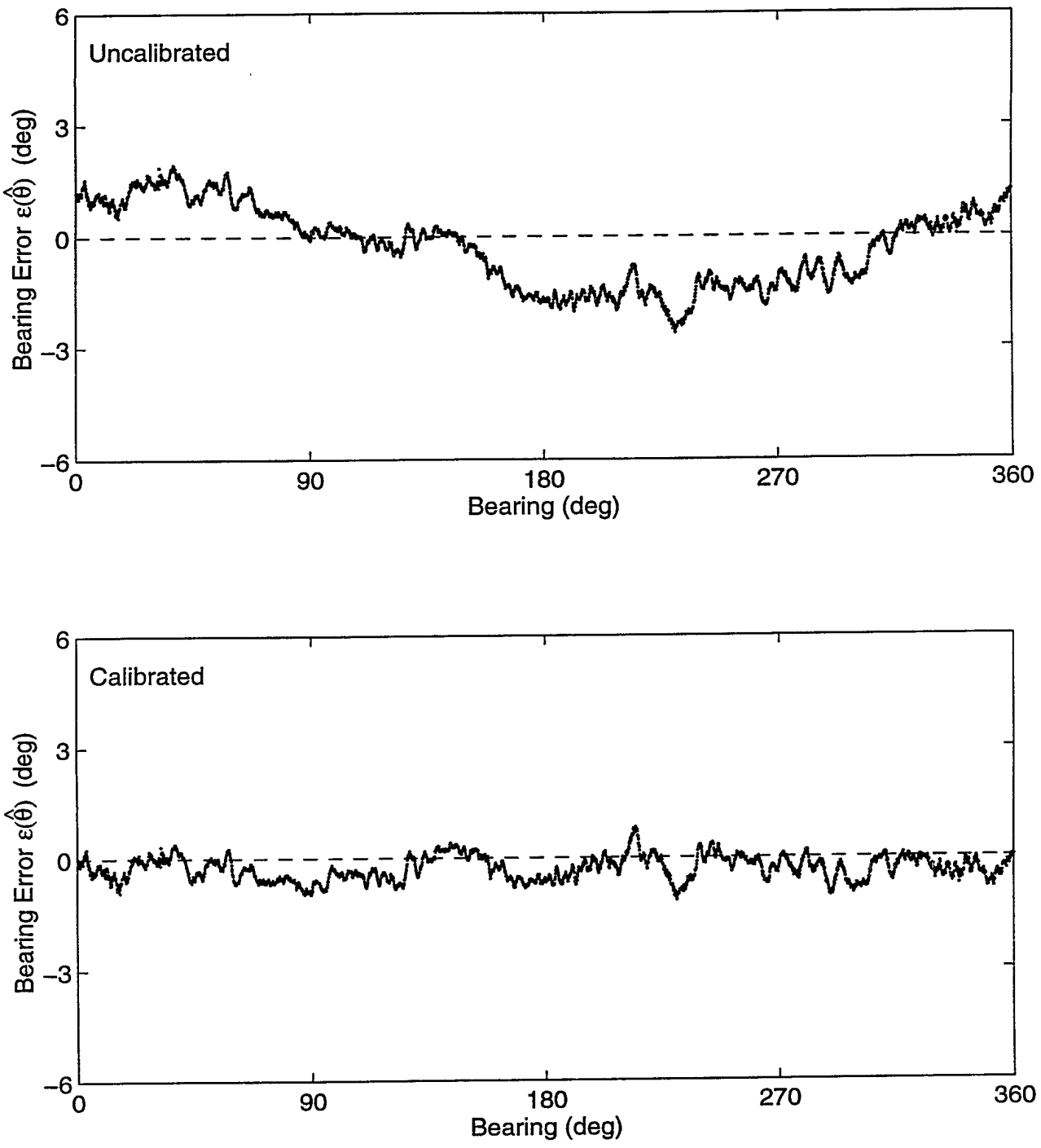

Figure 13. Errors in bearing estimates obtained with the data in File 1. The upper figure is calculated with the uncalibrated data and the lower figure is calculated with the calibrated data.

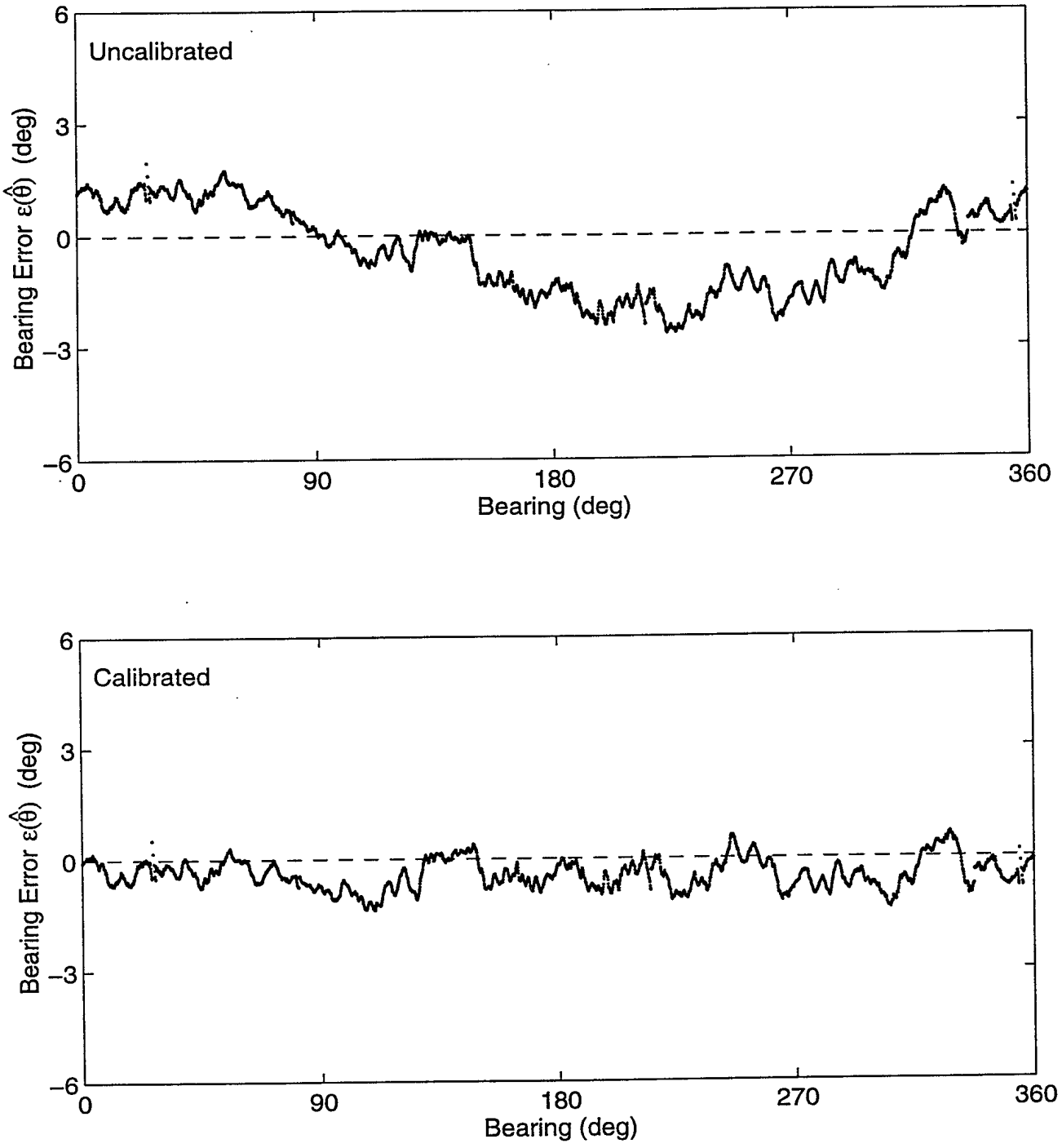

Figure 14. Errors in bearing estimates obtained with the data in File 2.

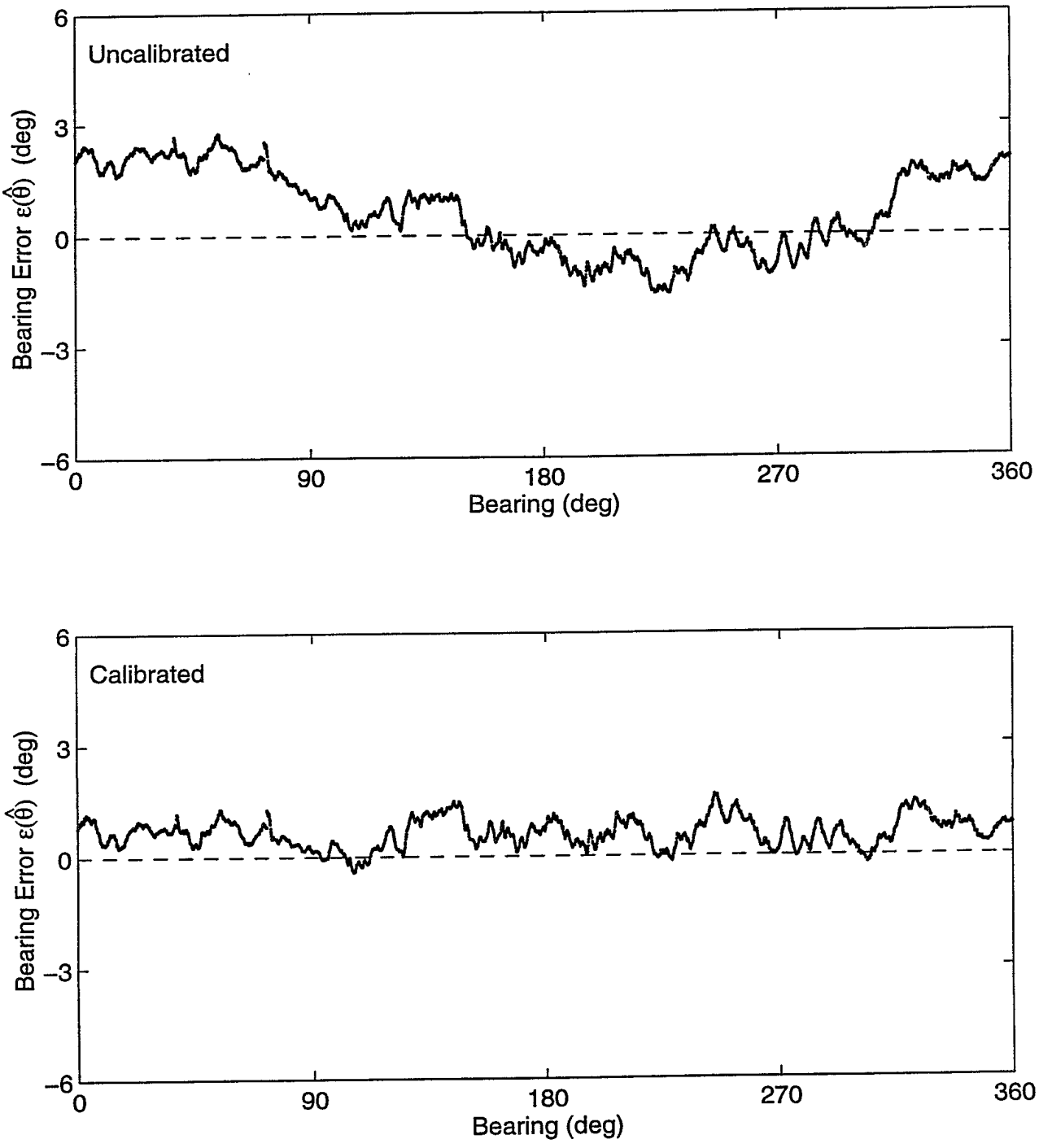

Figure 15. Errors in bearing estimates obtained with the data in File 3.

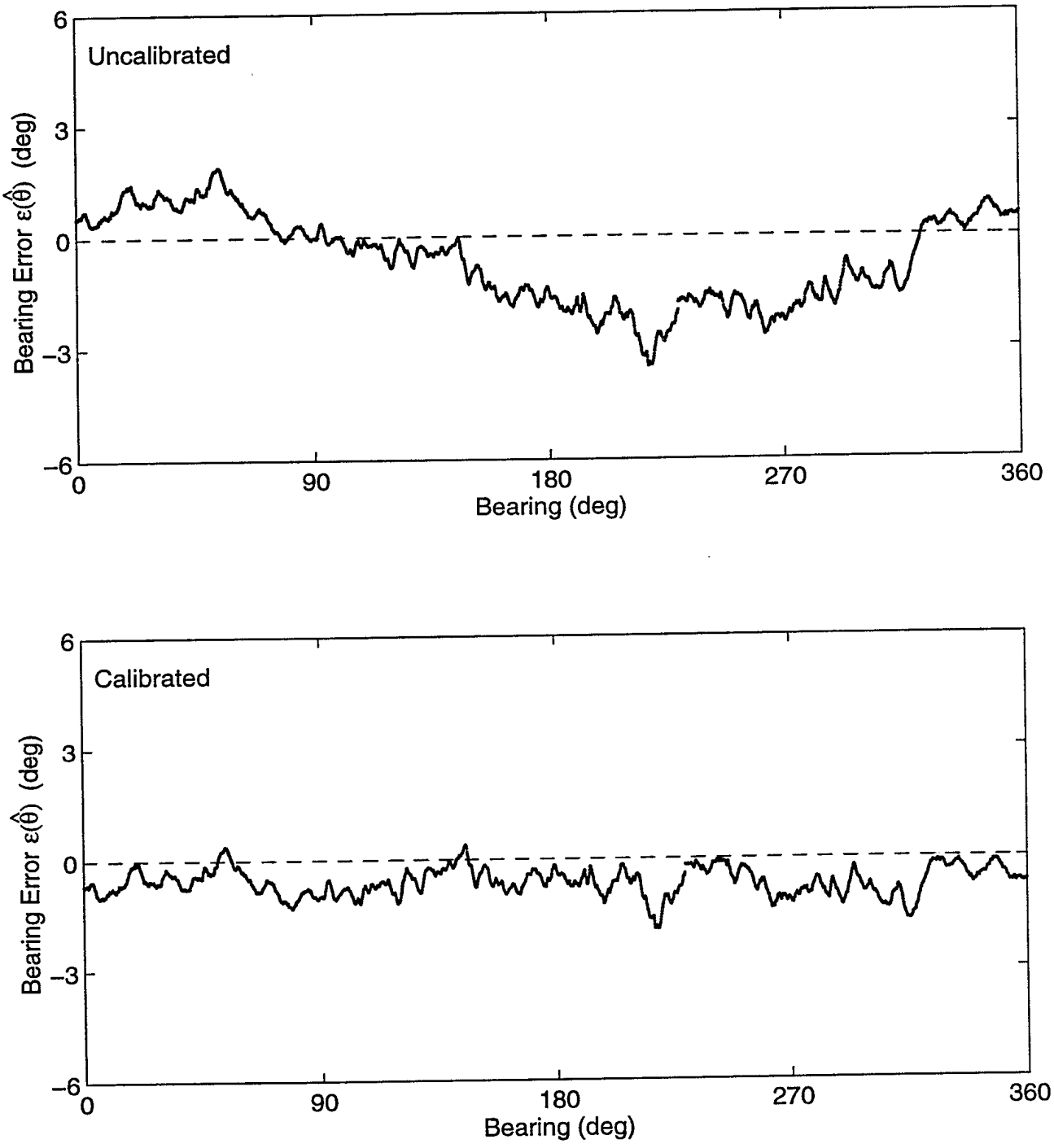

Figure 16. Errors in bearing estimates obtained with the data in File 4.

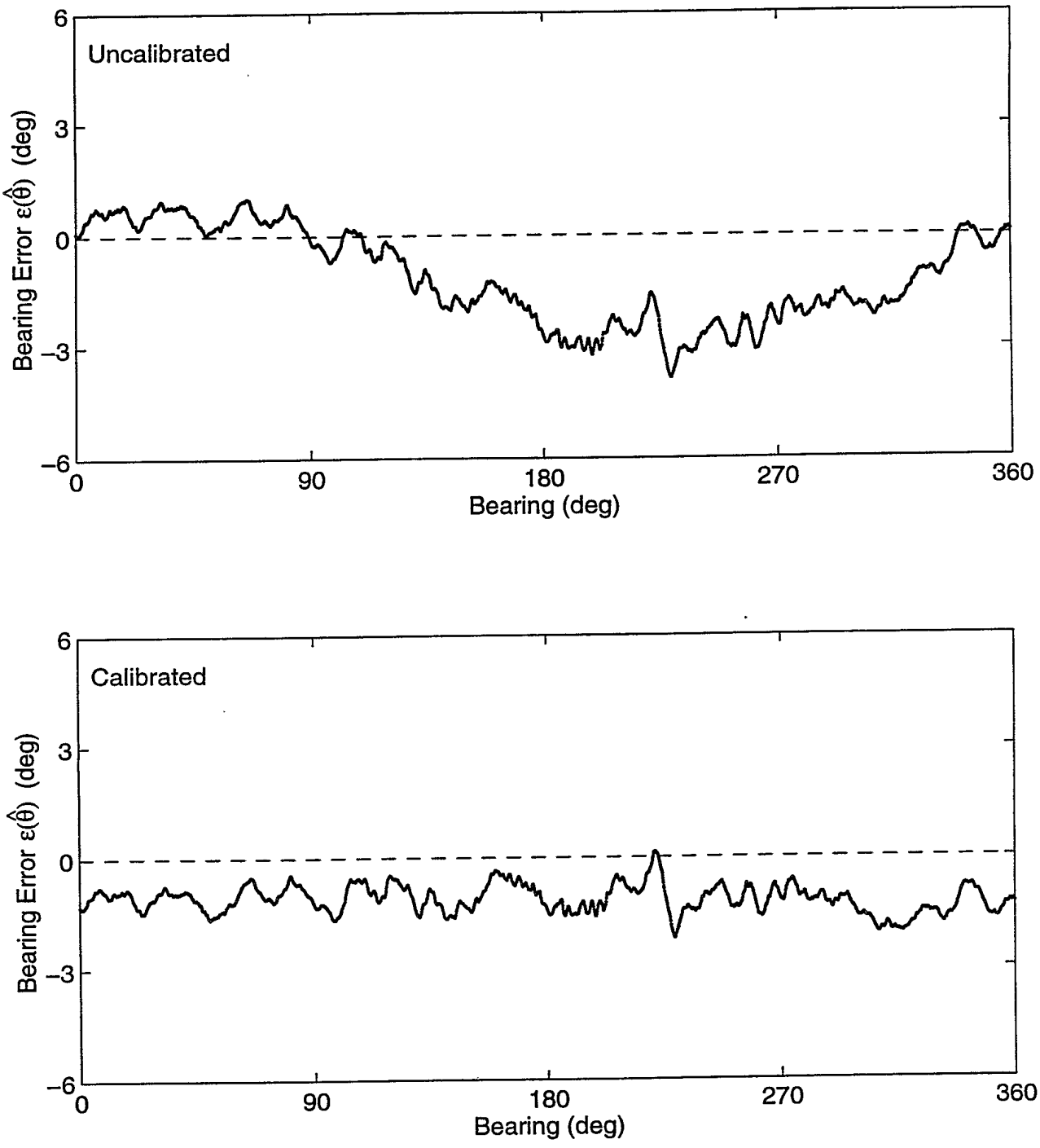

Figure 17. Errors in bearing estimates obtained with the data in File 5.

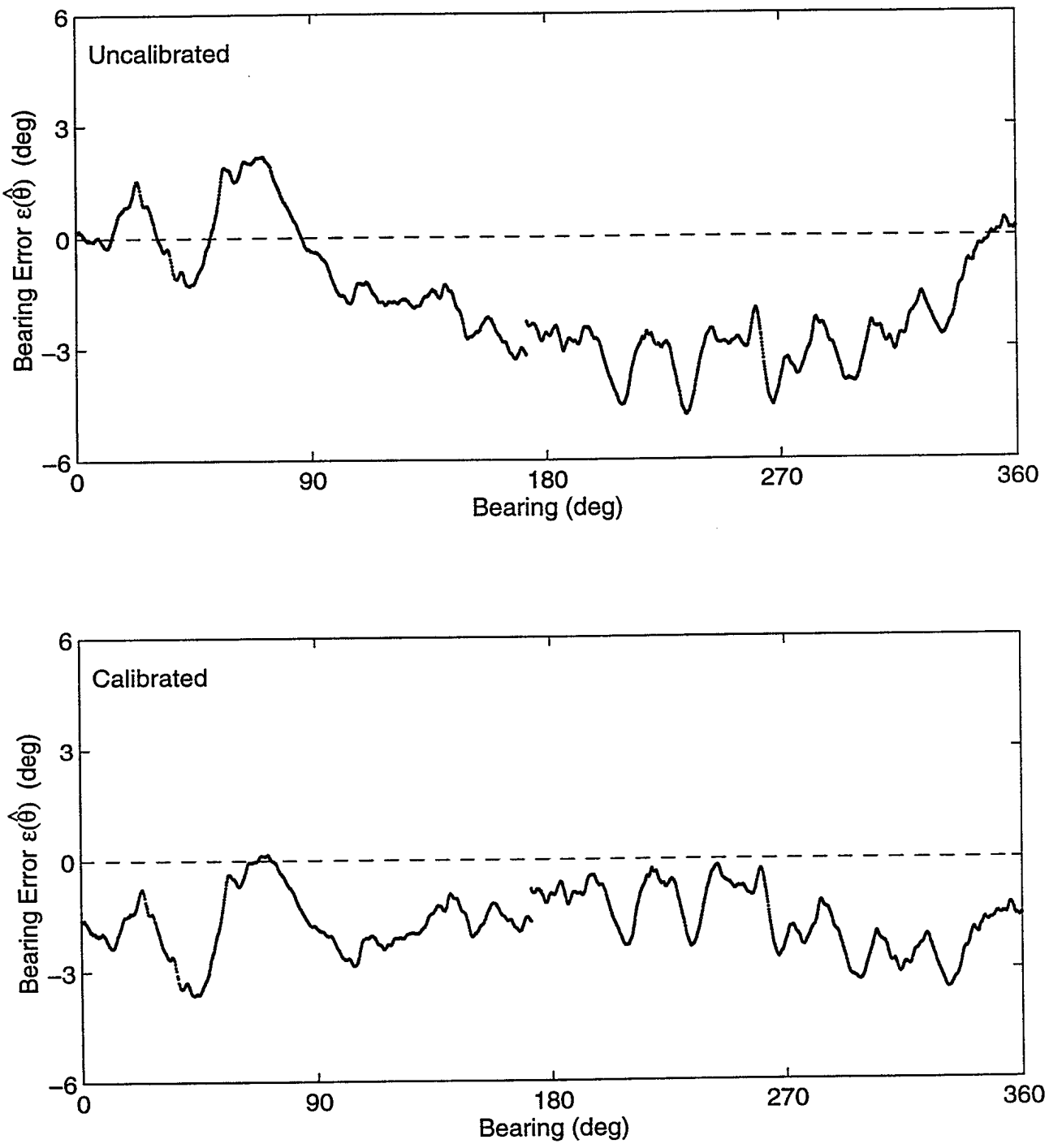

Figure 18. Errors in bearing estimates obtained with the data in File 6.

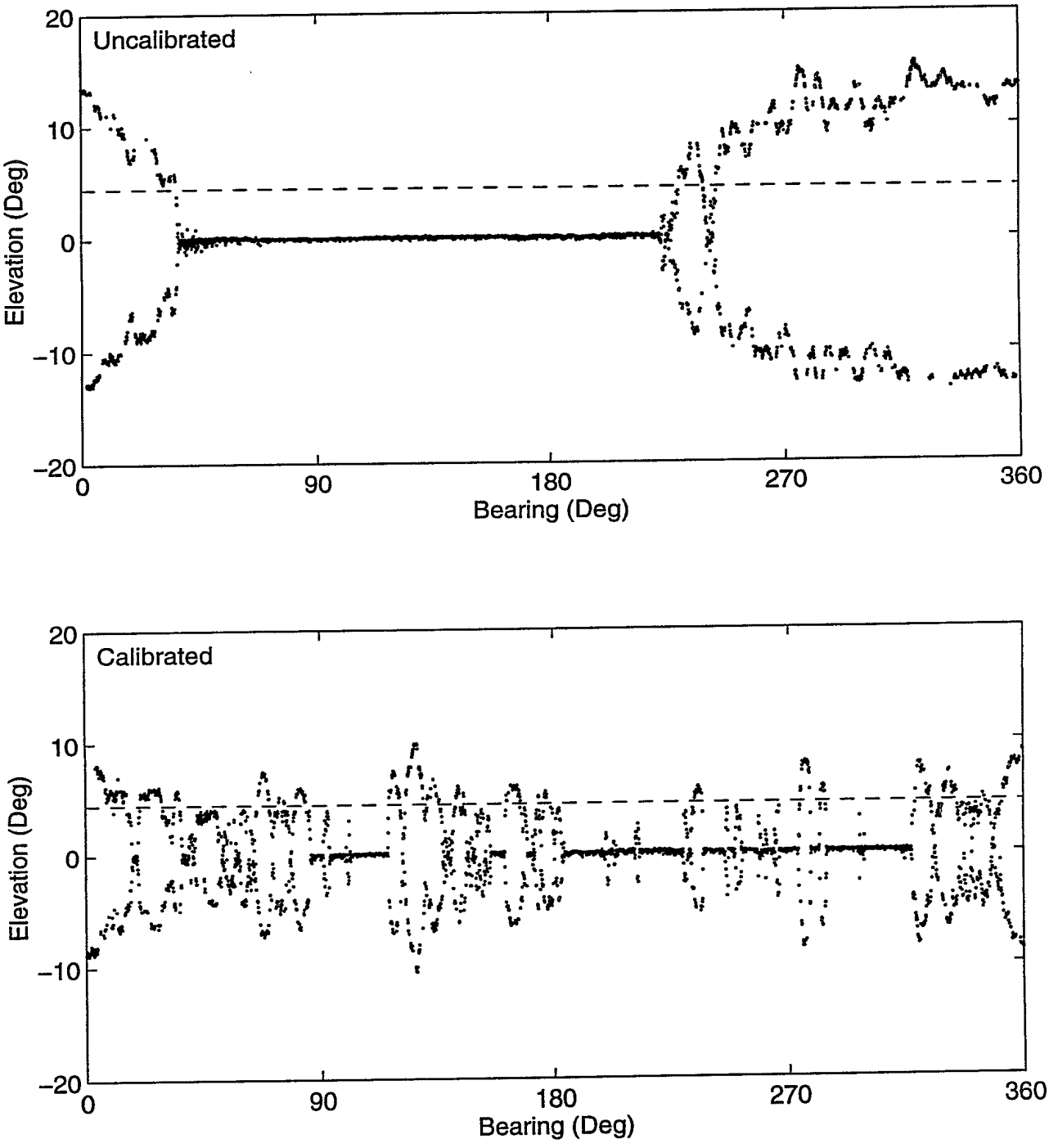

Figure 19. Elevation estimates obtained with the data in File 1.

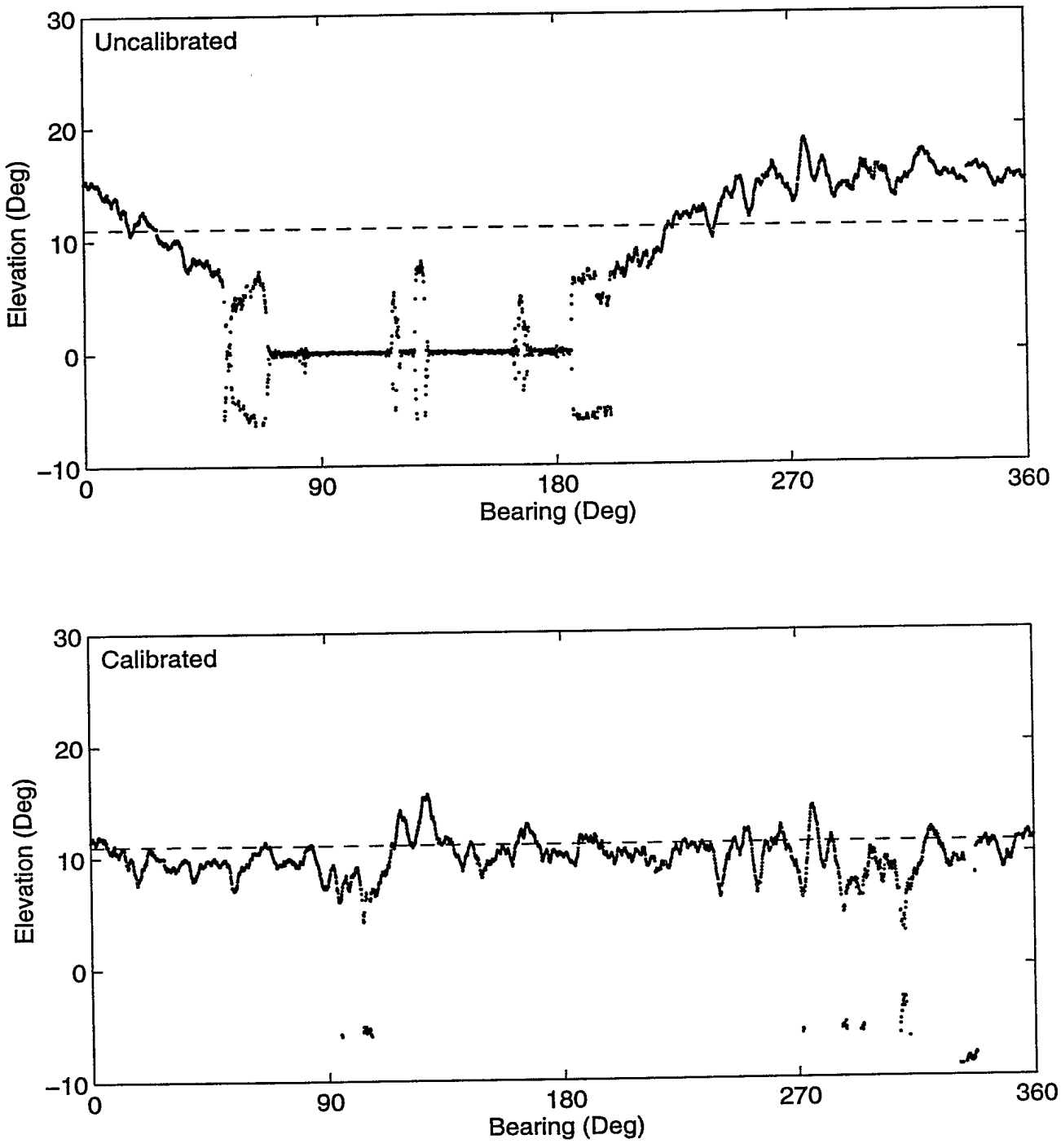

Figure 20. Elevation estimates obtained with the data in File 2.

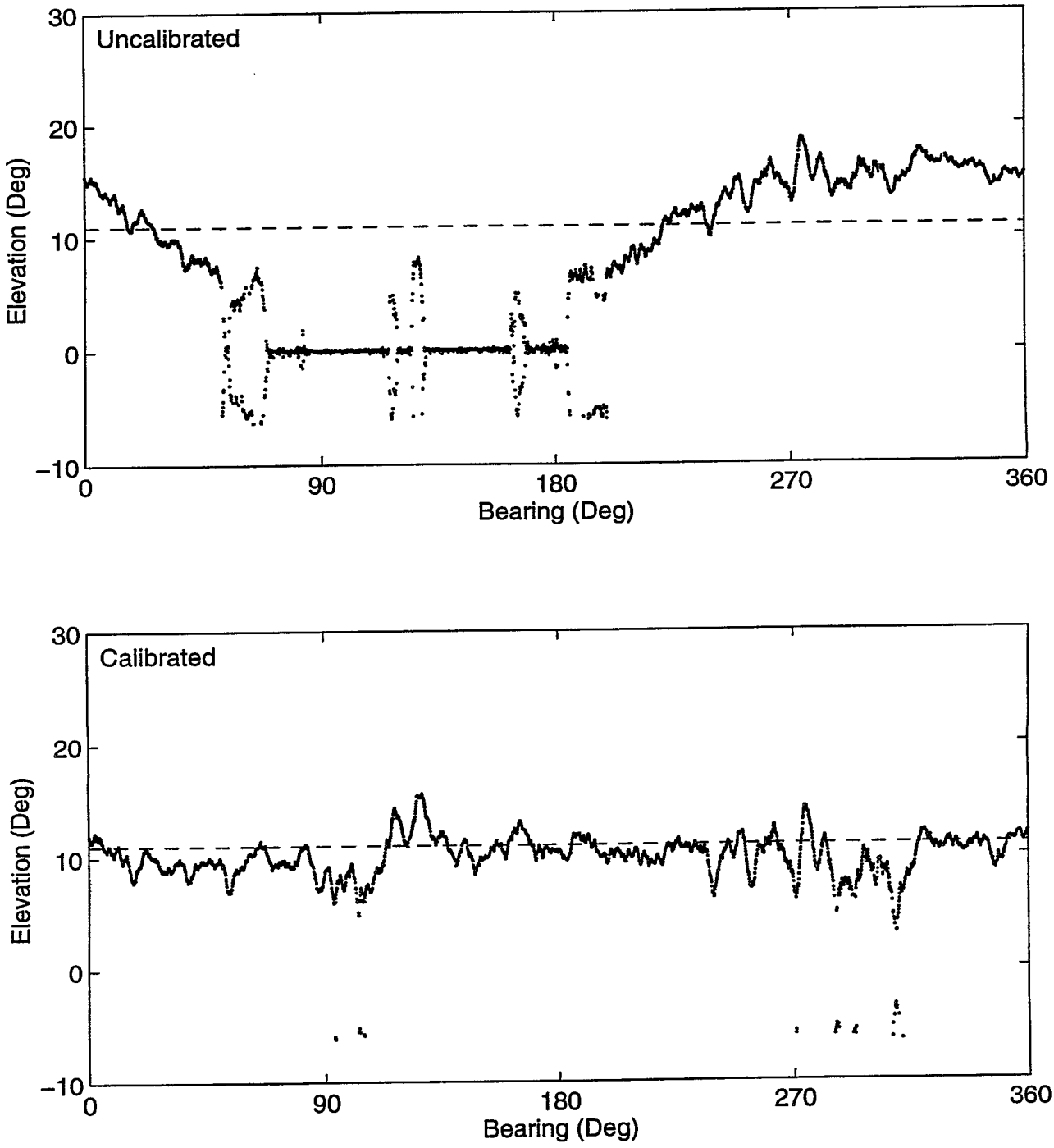

Figure 21. Elevation estimates obtained with the data in File 3.

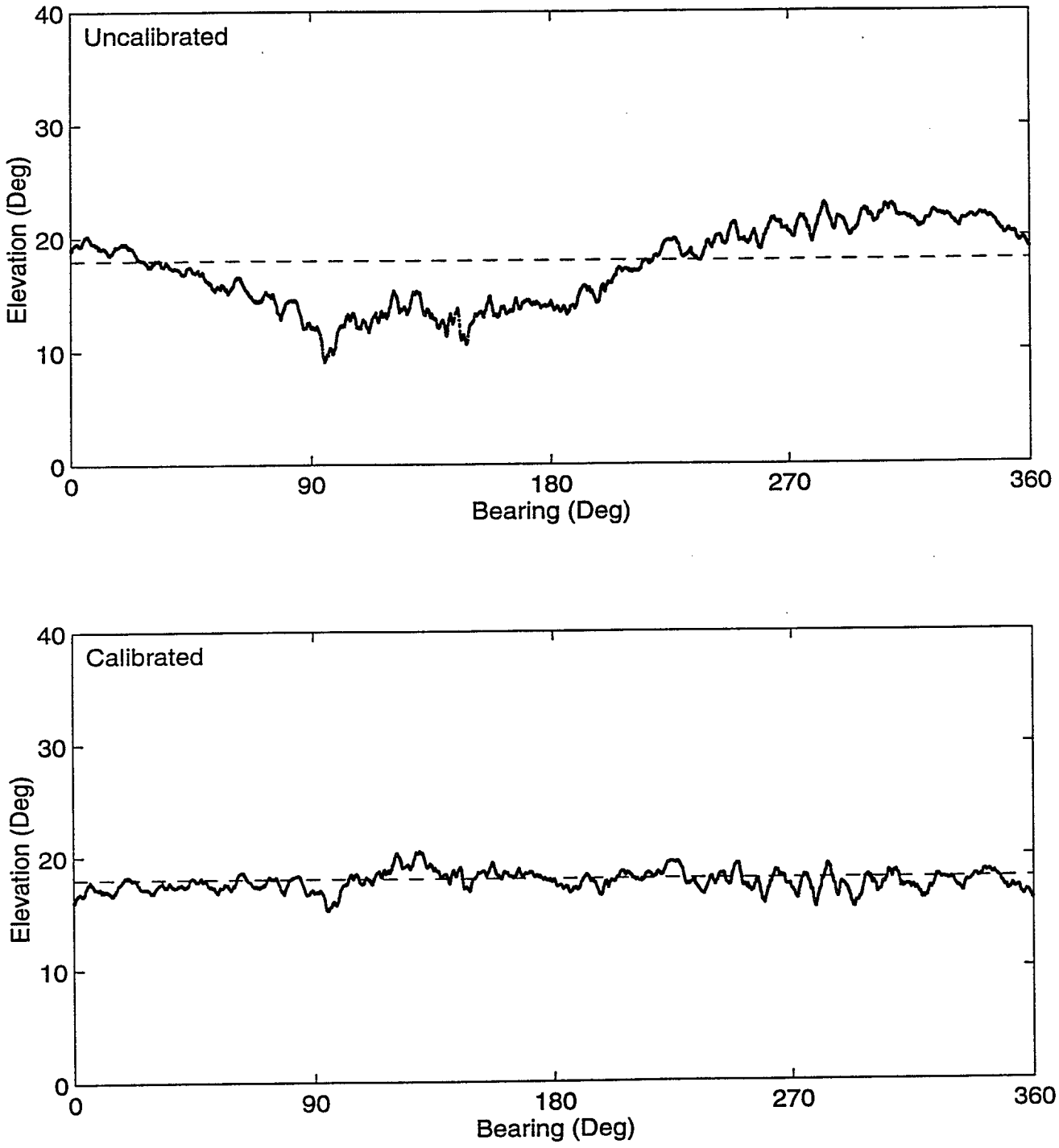

Figure 22. Elevation estimates obtained with the data in File 4.

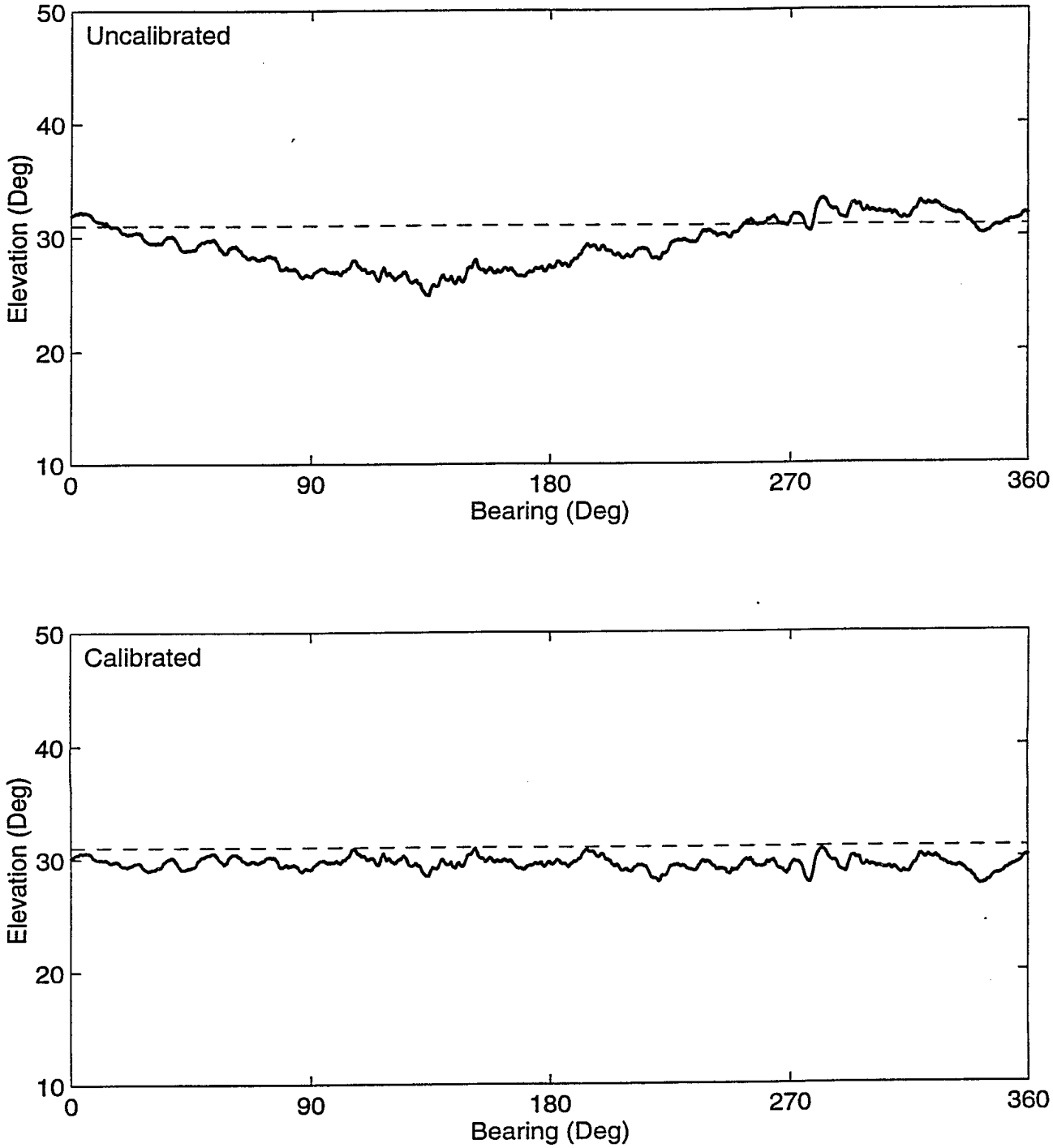

Figure 23. Elevation estimates obtained with the data in File 5.

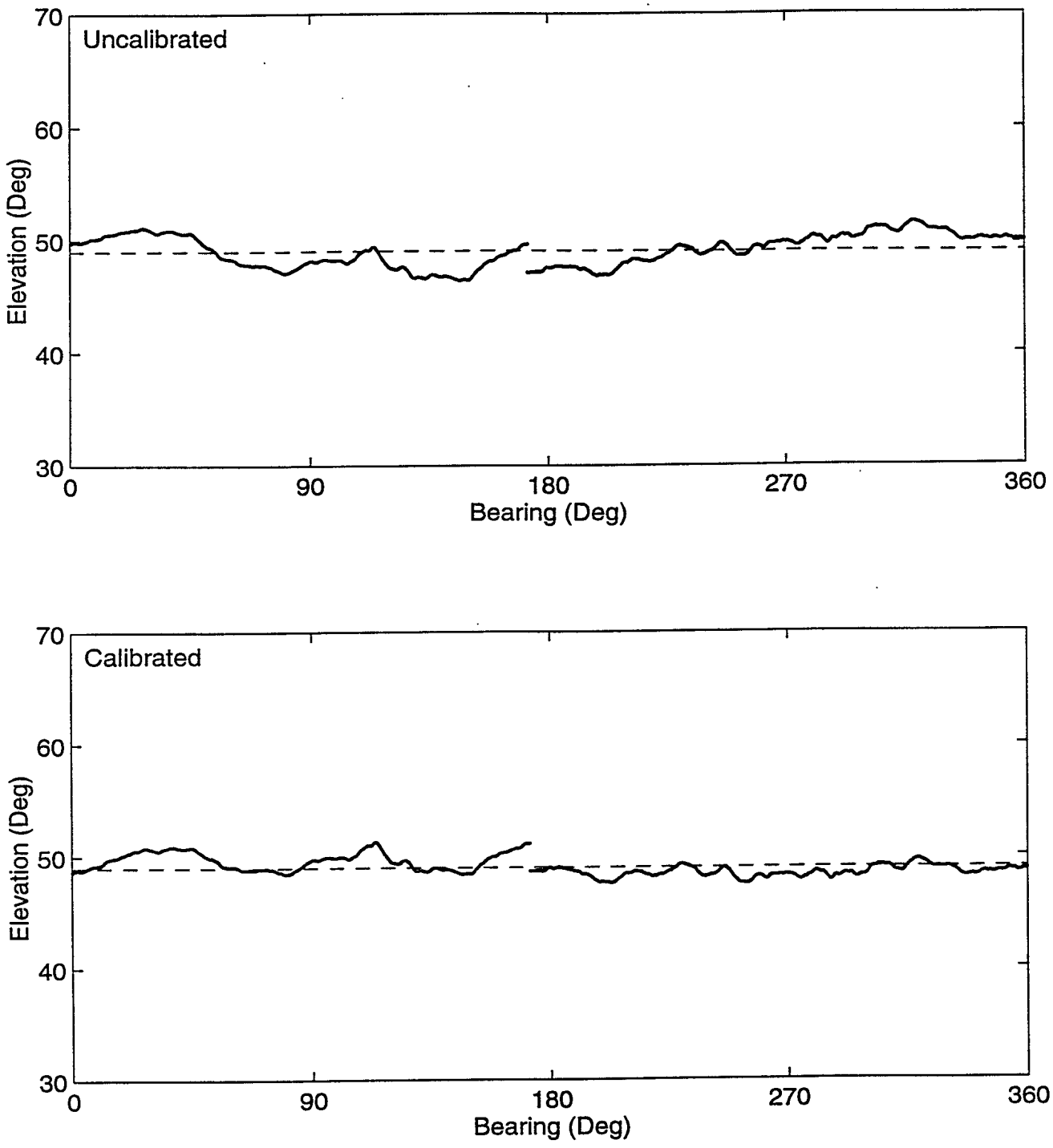

Figure 24. Elevation estimates obtained with the data in File 6.

7.2 Effect of Calibration on SINR

The calibration changes the SINR of transmitter signal in the array snapshots. This change reflects the effectiveness of the calibration method, because an increase in the SINR corresponds to a higher detection probability of the transmitter signal and a more accurate estimate of the signal direction. Here, the change is denoted by $SINR_C$ and is defined as the ratio

$$SINR_C = \frac{SINR_A}{SINR_B} , \tag{7.3}$$

where $SINR_A$ is the SINR after calibration and $SINR_B$ is the SINR before calibration.

We calculate $SINR_B$, the SINR before calibration, with an uncalibrated array snapshot $\mathbf{x}$ as

$$SINR_B = |\mathbf{x}_{/\!/}/\mathbf{x}_{\perp}|^2 = \frac{|\mathbf{x}^H \mathbf{a}(\hat{\theta}_t,\hat{\psi}_t)|^2}{|\mathbf{x}|^2|\mathbf{a}(\hat{\theta}_t,\hat{\psi}_t)|^2 - |\mathbf{x}^H \mathbf{a}(\hat{\theta}_t,\hat{\psi}_t)|^2} , \tag{7.4}$$

where $(\hat{\theta}_t,\hat{\psi}_t)$ is the estimate of the transmitter direction obtained from $\mathbf{x}$, $\mathbf{a}(\hat{\theta}_t,\hat{\psi}_t)$ is the array steering vector for this direction, $\mathbf{x}_{/\!/}$ is the component of $\mathbf{x}$ parallel to $\mathbf{a}(\hat{\theta}_t,\hat{\psi}_t)$, and $\mathbf{x}_{\perp}$ is the component of $\mathbf{x}$ perpendicular to $\mathbf{a}(\hat{\theta}_t,\hat{\psi}_t)$. The corresponding expression for $SINR_A$ is obtained by using $\mathbf{x}^c$ and $(\hat{\theta}_t^c,\hat{\psi}_t^c)$ instead of $\mathbf{x}$ and $(\hat{\theta}_t,\hat{\psi}_t)$, respectively. The justification for using the direction estimates is given in the Appendix. Note that the noise power in $SINR_B$ and $SINR_A$ refers to the noise power in the FFT bin where the largest signal is present. This bin has a bandwidth of 10.4 Hz.

Figures 25 to 30 contain the values of $SINR_A$, $SINR_B$ and $SINR_C$ calculated with the six files. For the sake of convenience in the

visual study of results, a horizontal 0-dB dashed line has been added to the figures for $SINR_C$. Some notable observations are given below:

1. The average value of $SINR_B$, the SINR before calibration, is between 16 and 17 dB in Files 1 to 5. It is approximately 15 dB in File 6.

   Remark: The smaller average value in File 6 is expected, because the transmitter elevation is the highest in this file and the element patterns are approximately dipoles with nulls in the vertical direction.

2. The average value of $SINR_C$, the change in SINR, is between 3 and 6 dB. The largest increases come from Files 2 and 3.

   Remark: This property agrees with the gain and phase estimates in Tables 3 and 4. The estimates obtained from File 2 are used to calibrate the array snapshots. They are essentially the same as the estimates from File 3. Therefore, one expects the largest increase in SINR to come from Files 2 and 3.

3. The SINRs in Figures 26 and 27, constructed with Files 2 and 3, are very similar.

   Remark: This property is also consistent with Observations 4 and 10 in Section 7.1.

4. In some figures, there are directions where the values of $SINR_C$ are slightly less than 0 dB, thus indicating that $SINR_A$ is slightly less than $SINR_B$.

   Remark: This result is not unexpected. The values of $SINR_A$ in these directions are not unusually low compared with those in

other directions. The negative values only indicate that original calibration coefficients are better for these directions.

Remark: The exceptions show that the calibration coefficients depend on signal directions.

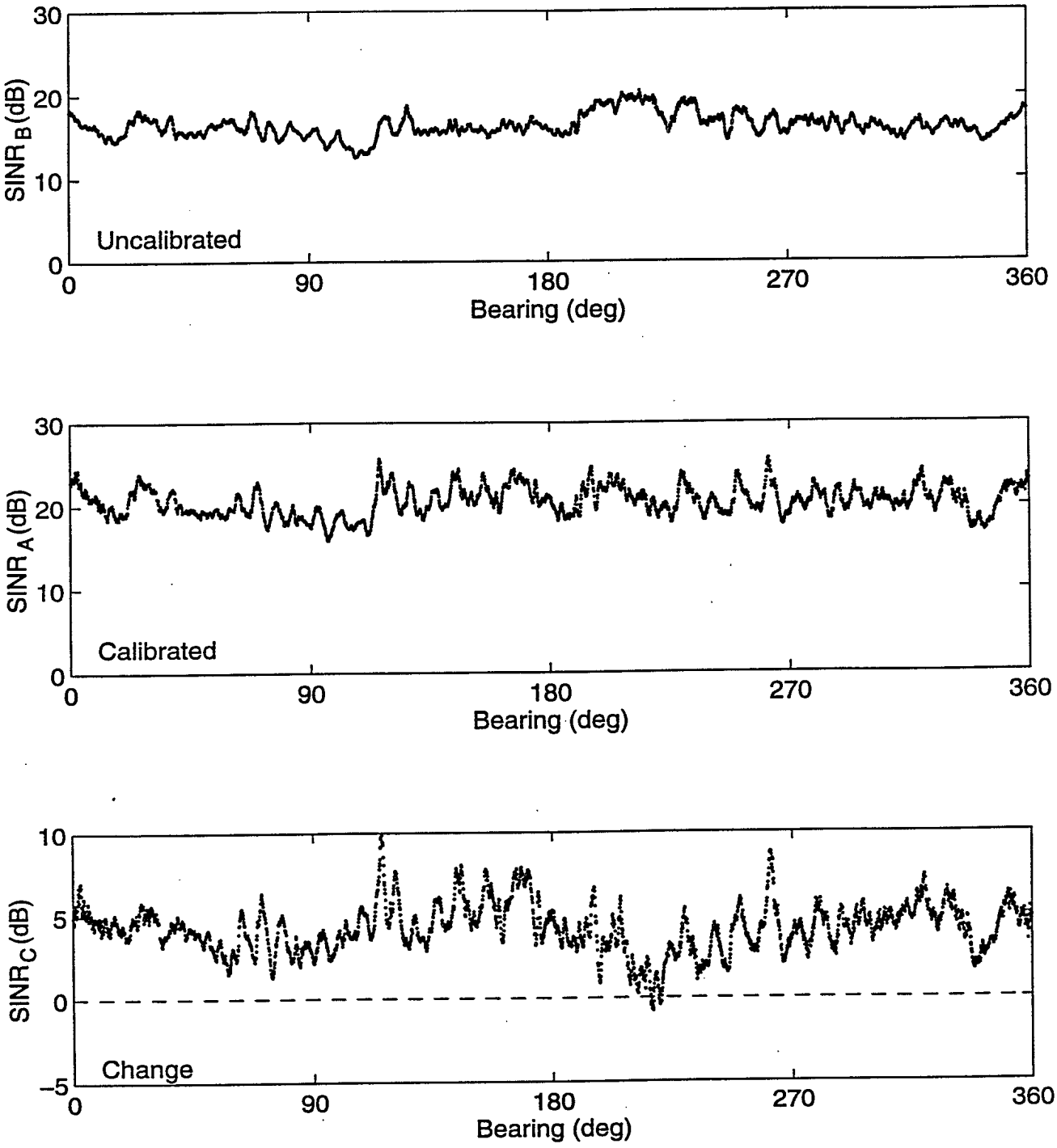

Figure 25. SINRs calculated before and after calibration and changes due to calibration, obtained with the data in File 1.

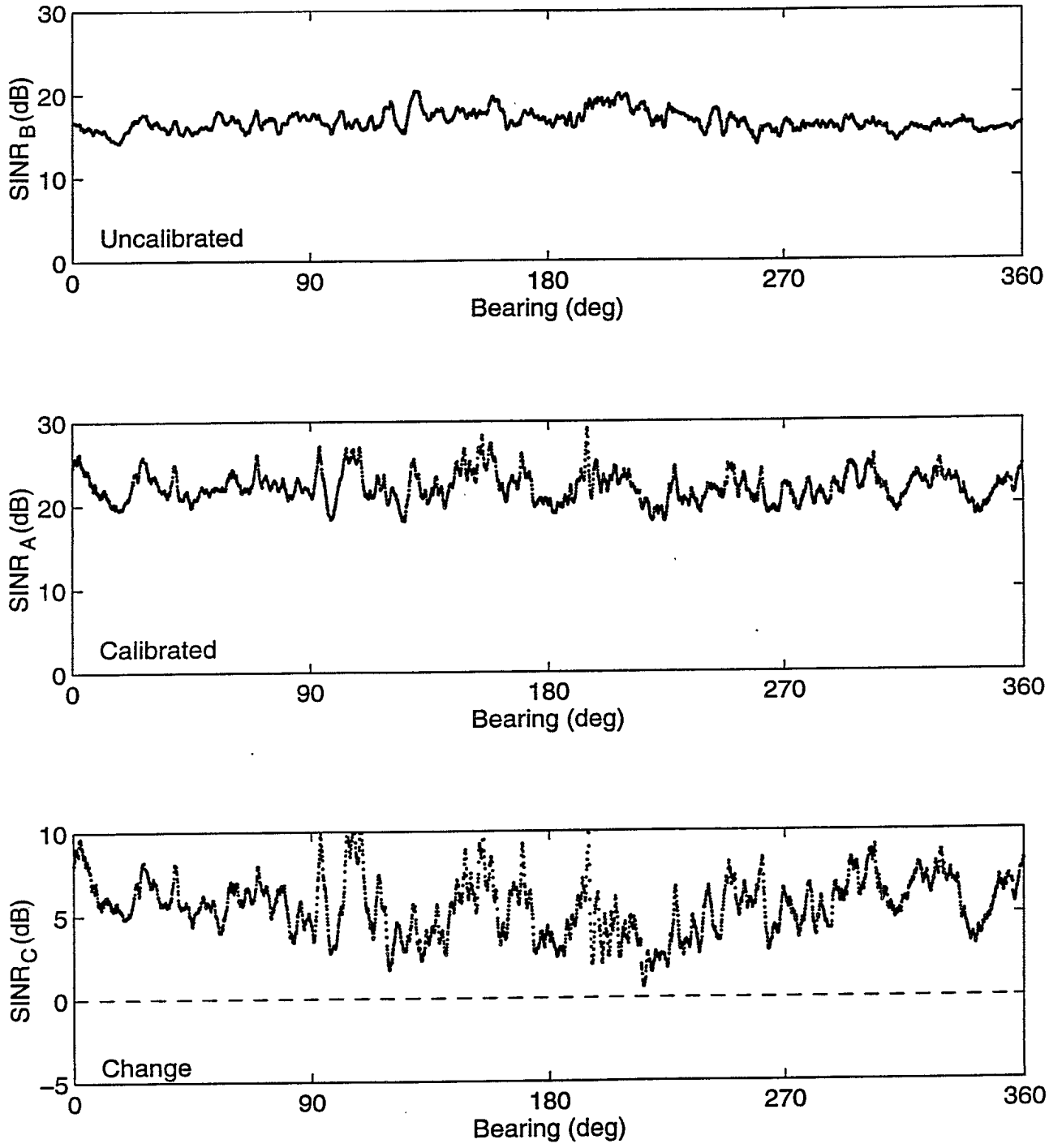

Figure 26. SINRs calculated before and after calibration and changes due to calibration, obtained with the data in File 2.

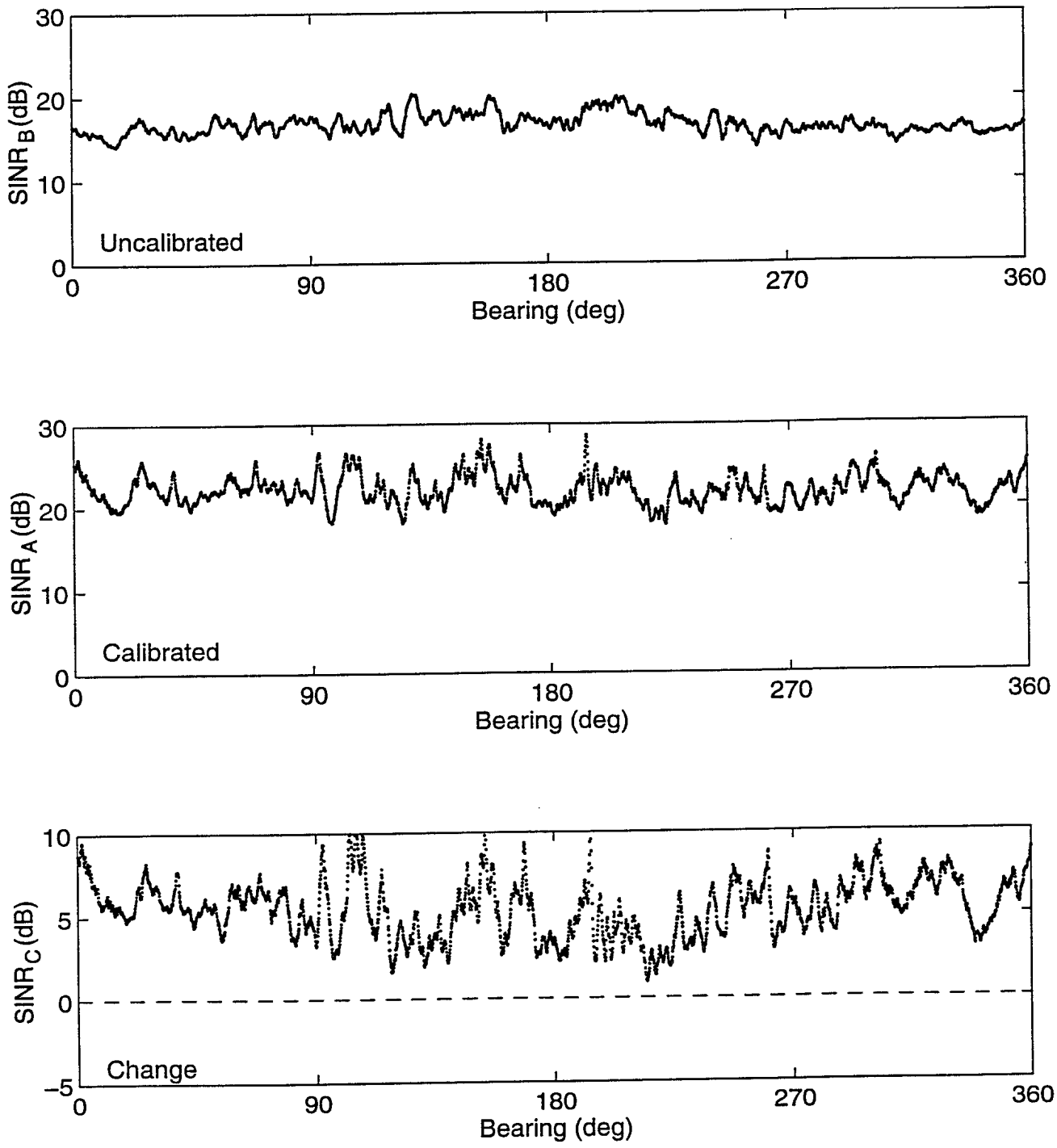

Figure 27. SINRs calculated before and after calibration and changes due to calibration, obtained with the data in File 3.

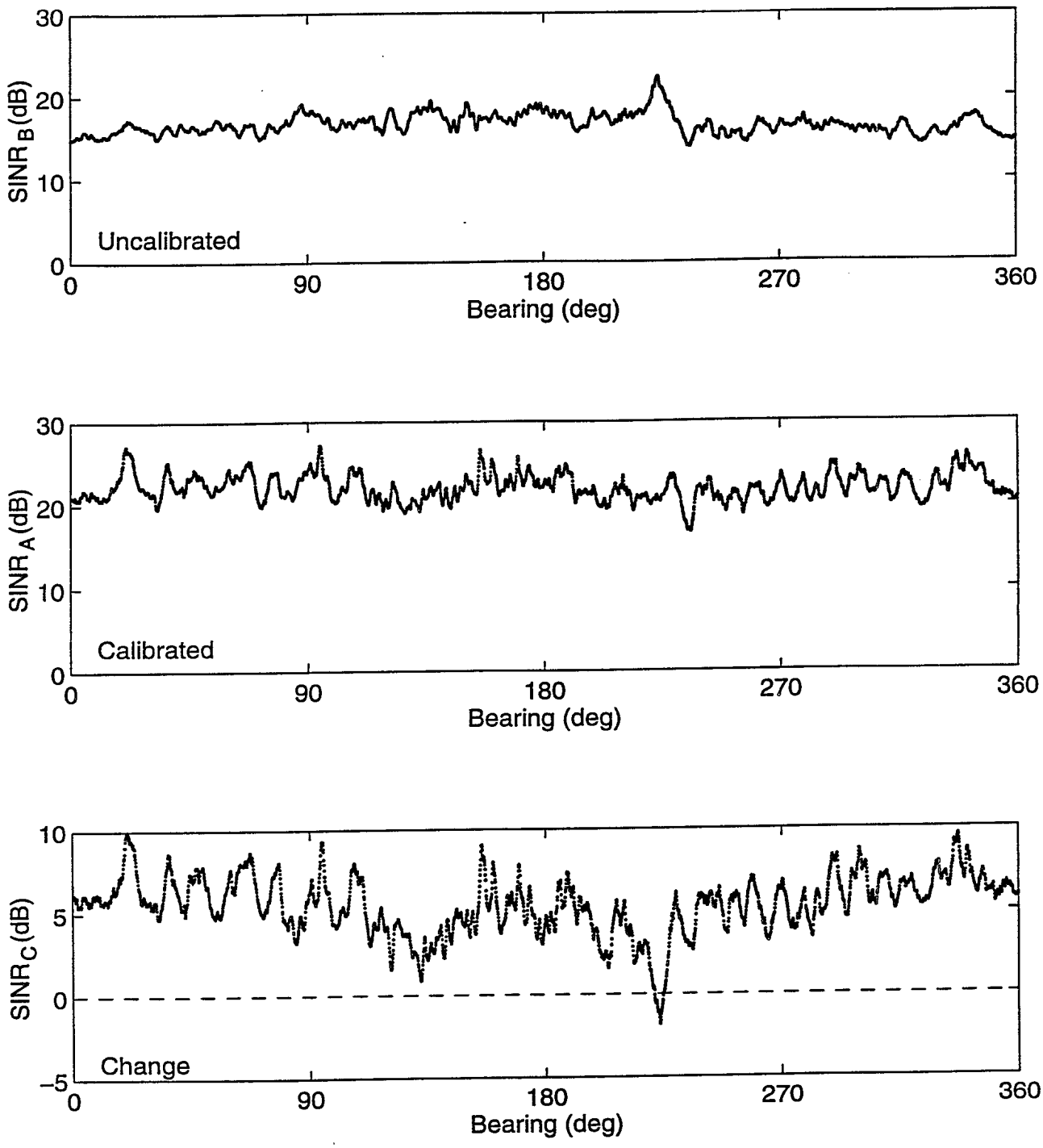

Figure 28. SINRs calculated before and after calibration and changes due to calibration, obtained with the data in File 4.

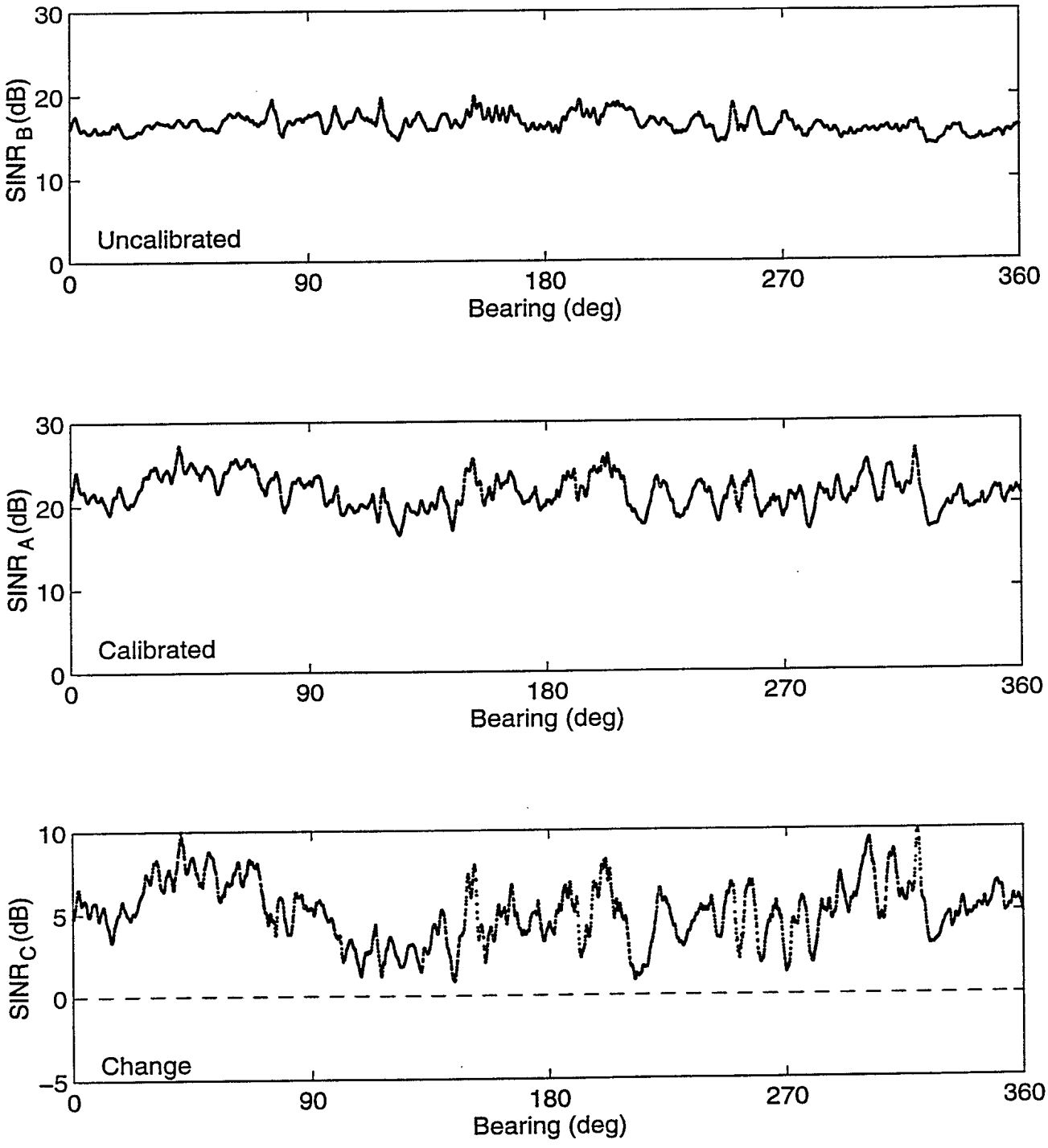

Figure 29. SINRs calculated before and after calibration and changes due to calibration, obtained with the data in File 5.

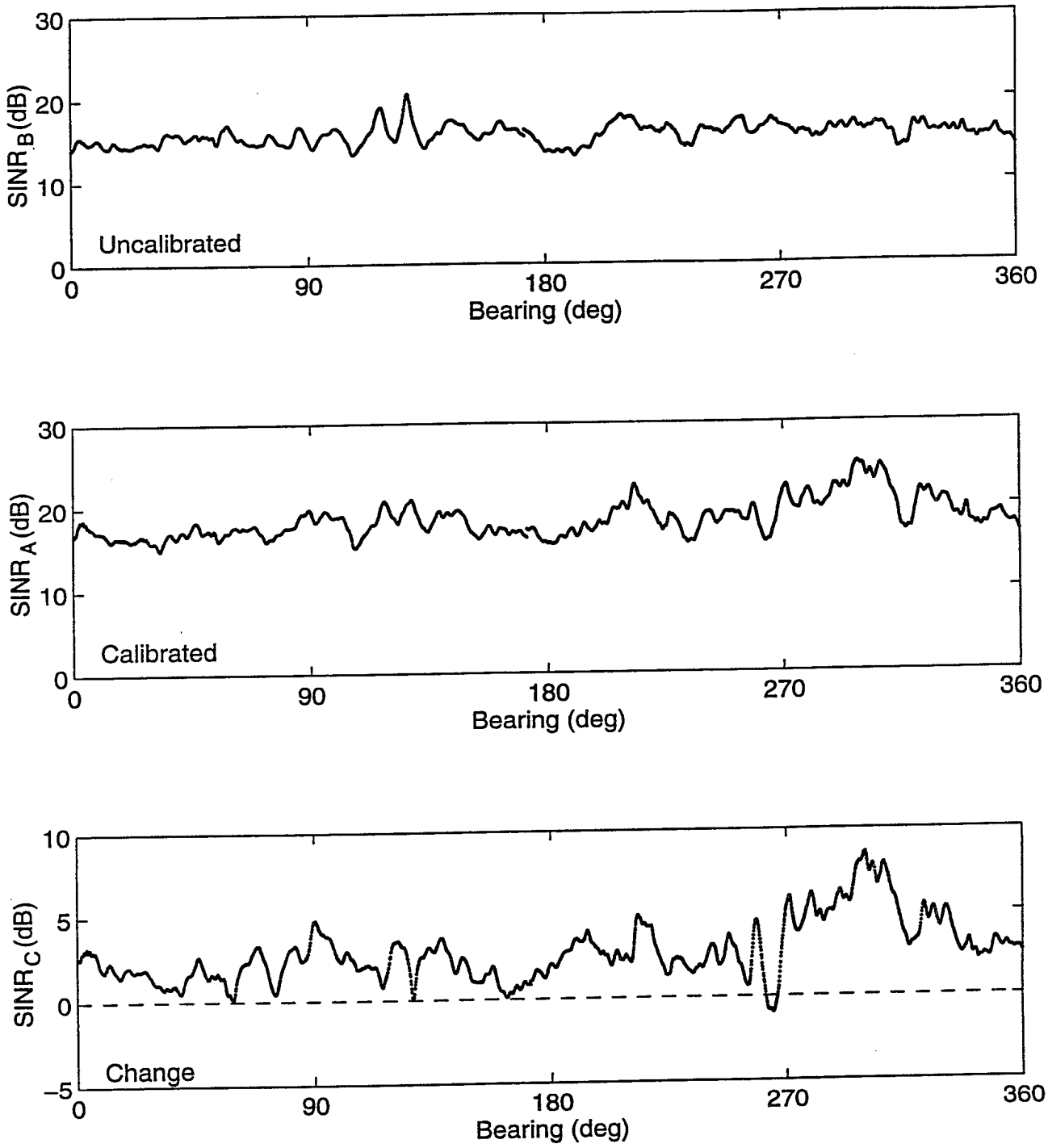

Figure 30. SINRs calculated before and after calibration and changes due to calibration, obtained with the data in File 6.

7.3 Resolution of Signal Directions

This study compares the resolution performance of the antenna array before and after calibration. It involves the construction of array snapshots with two signal sources present. The maximum likelihood method is used to estimate the two signal directions in these snapshots.

There are five steps in the procedure. Steps 1 extracts a section of 2K preprocessed array snapshots, $\{\mathbf{x}''_1, \mathbf{x}''_2, \mathbf{x}''_3, \cdots, \mathbf{x}''_{2K}\}$, from a file subset constructed in Section 6. This section is 60° wide in bearing and is such that the transmitter bearing is between (θ"-30°) and (θ"+30°), where θ" is the centre of the region where bearing resolution is studied. Step 2 separates this section into two groups: $\{\mathbf{x}''_1, \mathbf{x}''_3, \mathbf{x}''_5, \cdots, \mathbf{x}''_{2K-1}\}$ and $\{\mathbf{x}''_{2K}, \mathbf{x}''_{2K-2}, \mathbf{x}''_{2K-4}, \cdots, \mathbf{x}''_2\}$. In the first group, the transmitter bearing increases from (θ"-30°) to (θ"+30°). In the second, the order of the snapshots is reversed to make the bearing decrease from (θ"+30°) to (θ"-30°). These groups are then combined to form a new set $\{\mathbf{y}_1, \mathbf{y}_2, \mathbf{y}_3, \cdots, \mathbf{y}_K\}$, in which there are two signal sources crossing each other at the bearing θ". In Step 4, (7.6) is obtained from (7.1) by using y_{kn} and y^c_{kn} instead of x_n and x^c_n, respectively. The details are given below:

Step 1.

Extracts a section of 2K snapshots from a specified file subset. Identify its snapshots as $\{\mathbf{x}''_1, \mathbf{x}''_2, \mathbf{x}''_3, \cdots, \mathbf{x}''_{2K}\}$.

Step 2.

Construct a set of K new snapshots $\{\mathbf{y}_1, \mathbf{y}_2, \mathbf{y}_3, \cdots, \mathbf{y}_K\}$ as

$$\mathbf{y}_k = \mathbf{x}''_{2k-1} + \mathbf{x}''_{2K+2-2k}, \qquad k=1,2,3,\ldots,K . \tag{7.5}$$

Step 3.

Use the maximum likelihood method to estimate two signal directions from each snapshot in $\{\mathbf{y}_1, \mathbf{y}_2, \mathbf{y}_3, \cdots, \mathbf{y}_K\}$. Denote the estimates obtained from $\mathbf{y}_k$ by $\{\hat{\theta}_{k1}, \hat{\psi}_{k1}\}$ and $\{\hat{\theta}_{k2}, \hat{\psi}_{k2}\}$.

Step 4.

Construct a set of K calibrated snapshots $\{\mathbf{y}_1^c, \mathbf{y}_2^c, \mathbf{y}_3^c, \cdots, \mathbf{y}_K^c\}$ as

$$y_{kn}^c = \hat{g}_n^{-1} \exp[-j\hat{\phi}_n]\ y_{kn}\ , \qquad n=1,2,\cdots,N\ . \qquad (7.6)$$

Step 5.

Use the maximum likelihood method to estimate two signal directions from each snapshot in $\{\mathbf{y}_1^c, \mathbf{y}_2^c, \mathbf{y}_3^c, \cdots, \mathbf{y}_K^c\}$. Denote the estimates from $\mathbf{y}_k^c$ by $\{\hat{\theta}_{k1}^c, \hat{\psi}_{k1}^c\}$ and $\{\hat{\theta}_{k2}^c, \hat{\psi}_{k2}^c\}$.

This study uses $\theta"=30°$, K=300 for Files 1 to 5, and K=170 for File 6. The value of $\theta"$ corresponds to a bearing where the azimuth aperture of the array is the smallest. Consequently, the bearing beamwidth is the largest and the changes in bearing resolution are easiest to observe. The values of K are determined by the file sizes.

Figures 31 to 36 contain the bearing estimates $\hat{\theta}_{k1}$, $\hat{\theta}_{k2}$, $\hat{\theta}_{k1}^c$, and $\hat{\theta}_{k2}^c$ obtained. These estimates are plotted in point mode. Each figure has two solid lines. They are GPS tracks calculated with (3.2) and $\Delta'=7.4$ seconds. One GPS track is the source track in $\{\mathbf{x}"_1, \mathbf{x}"_3, \mathbf{x}"_5, \cdots, \mathbf{x}"_{2K-1}\}$. The other is the source track in $\{\mathbf{x}"_{2K}, \mathbf{x}"_{2K-2}, \mathbf{x}"_{2K-4}, \cdots, \mathbf{x}"_2\}$. There are several notable observations:

1. In each figure, the bearing estimates cluster around two imaginary lines that intersect at bearing $\theta"$.

2. The imaginary lines deviate from the solid lines. The calibration reduces these deviations in the results from Files

1 to 4.

3. The scattering of the points about the imaginary lines is generally larger if the angular separation of the true signal bearings is smaller.

   Remark: This property is expected, because it is more difficult to resolve two signal directions if these directions are closer togther. More difficulty in resolution also leads to larger errors in the estimates.

4. The calibration reduces the scattering of the bearing estimates obtained with Files 1 to 5.

We also quantify resolution performance with the technique described below. It should be noted that $SINR_B$ is at least 15 dB in each snapshot in the set $\{\mathbf{x}''_1, \mathbf{x}''_3, \mathbf{x}''_5, \cdots, \mathbf{x}''_{2K-1}\}$ (Observation 1, page 55); the $SINR_A$ in the each calibrated snapshots is higher (Observation 2, page 55); the array aperture for $\theta''=30°$ and zero elevation is approximately 113 meters; the signal wavelength at 5.1 MHz is 58.8 meters; and the azimuth beamwidth of the array is approximately 30°. Therefore, one can say that the signals in $\mathbf{y}_k$, for example, are not resolved if $\hat{\theta}_{k1}$ or $\hat{\theta}_{k2}$ is more than 15° from θ_{k1} and θ_{k2}. Here, θ_{k1} and θ_{k2} are the GPS directions in $\mathbf{x}''_{2k-1}$ and $\mathbf{x}''_{2K+2-2k}$, respectively, and are calculated with (3.2) and $\Delta'=7.4$ second. From (7.5), $\mathbf{x}''_{2k-1}$ and $\mathbf{x}''_{2K+2-2k}$ are the snapshots used to construct $\mathbf{y}_k$.

In the procedure below, J_B and J_A are the number of snapshots with unresolved signal directions. The subscripts 'B' and 'A' indicate before and after calibration, respectively.

Step 1.

Let $J_B=0$

Step 2.

Do for k=1 to K

Increase J_B by unity if

$$\{|\hat{\theta}_{k1}-\theta_{k1}| > 15° \text{ and } |\hat{\theta}_{k1}-\theta_{k2}| > 15°\}$$

or

$$\{|\hat{\theta}_{k2}-\theta_{k1}| > 15° \text{ and } |\hat{\theta}_{k2}-\theta_{k2}| > 15°\}.$$

End do

Step 3.

Let $J_A=0$

Step 4.

Do for k=1 to K

Increase J_A by unity if

$$\{|\hat{\theta}^c_{k1}-\theta_{k1}| > 15° \text{ and } |\hat{\theta}^c_{k1}-\theta_{k2}| > 15°\}$$

or

$$\{|\hat{\theta}^c_{k2}-\theta_{k1}| > 15° \text{ and } |\hat{\theta}^c_{k2}-\theta_{k2}| > 15°\}.$$

End do

The values of J_B and J_A thus obtained are in Rows 4 and 5 of Table 7, respectively. Rows 6 contains the percentage reduction (PR) in the number of unresolved snapshots, i.e.,

$$PR = \frac{100\ (J_B - J_A)}{J_B}\ \%. \qquad (7.7)$$

The following are some of the observations in addition to those derived from Figures 31 to 36.

5. The calibration improves the resolution performance of the antenna array in Files 1 to 5. There is a deterioration in resolution performance in File 6.

6. The values of PR for Files 1 to 3 are between 56 and 60%. Those for Files 4 and 5 are significantly smaller. In the case of File 6, PR is negative, because there are more unresolved signals after calibration.

   Remark: This dependence of PR on file is not unexpected. It was noted earlier in this section that there are perturbations in the gain and phase responses of the array elements and that these perturbations are larger if the transmitter range is shorter or if the transmitter elevation is higher. The range is the shortest and the elevation is the highest in File 6. Therefore, the poor results from File 6 are not unexpected.

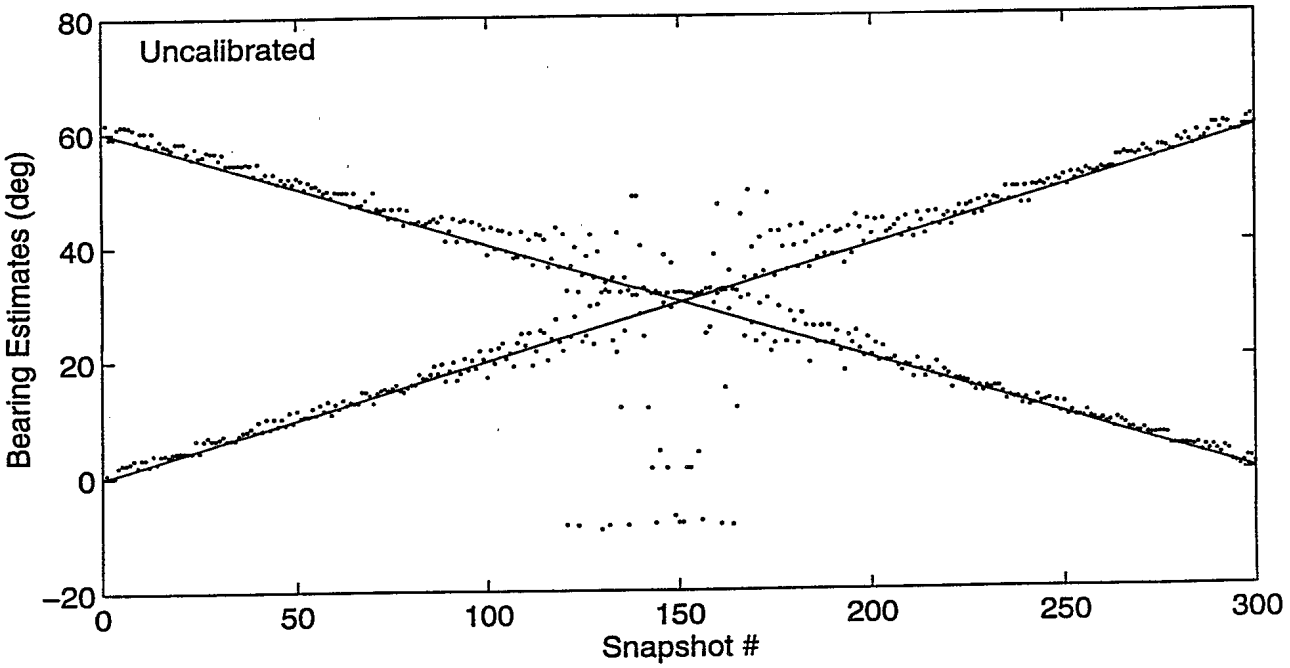

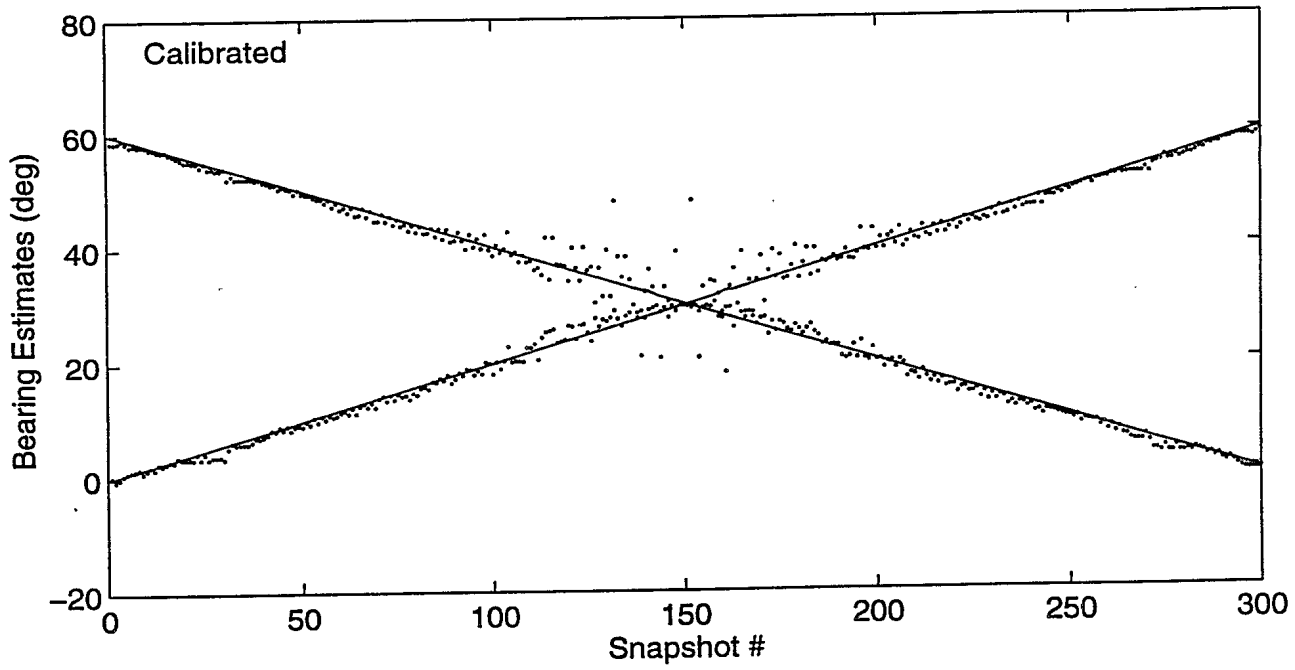

Figure 31. Bearing estimates (points) calculated with the data in File 1. The solid lines represent the true signal tracks calculated with (3.2) and Δ'=7.4 seconds.

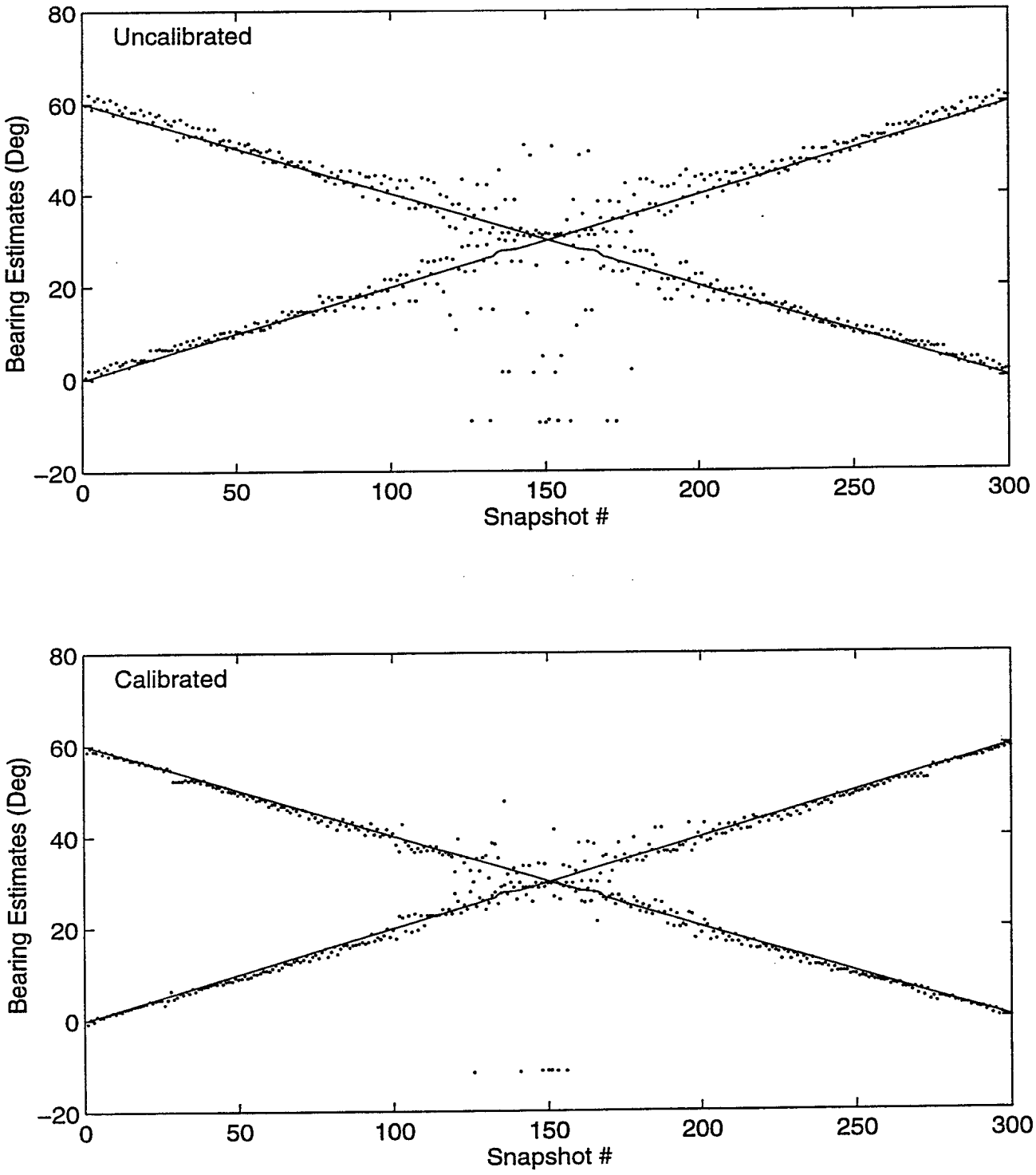

Figure 32. Bearing estimates (points) calculated with the data in File 2.

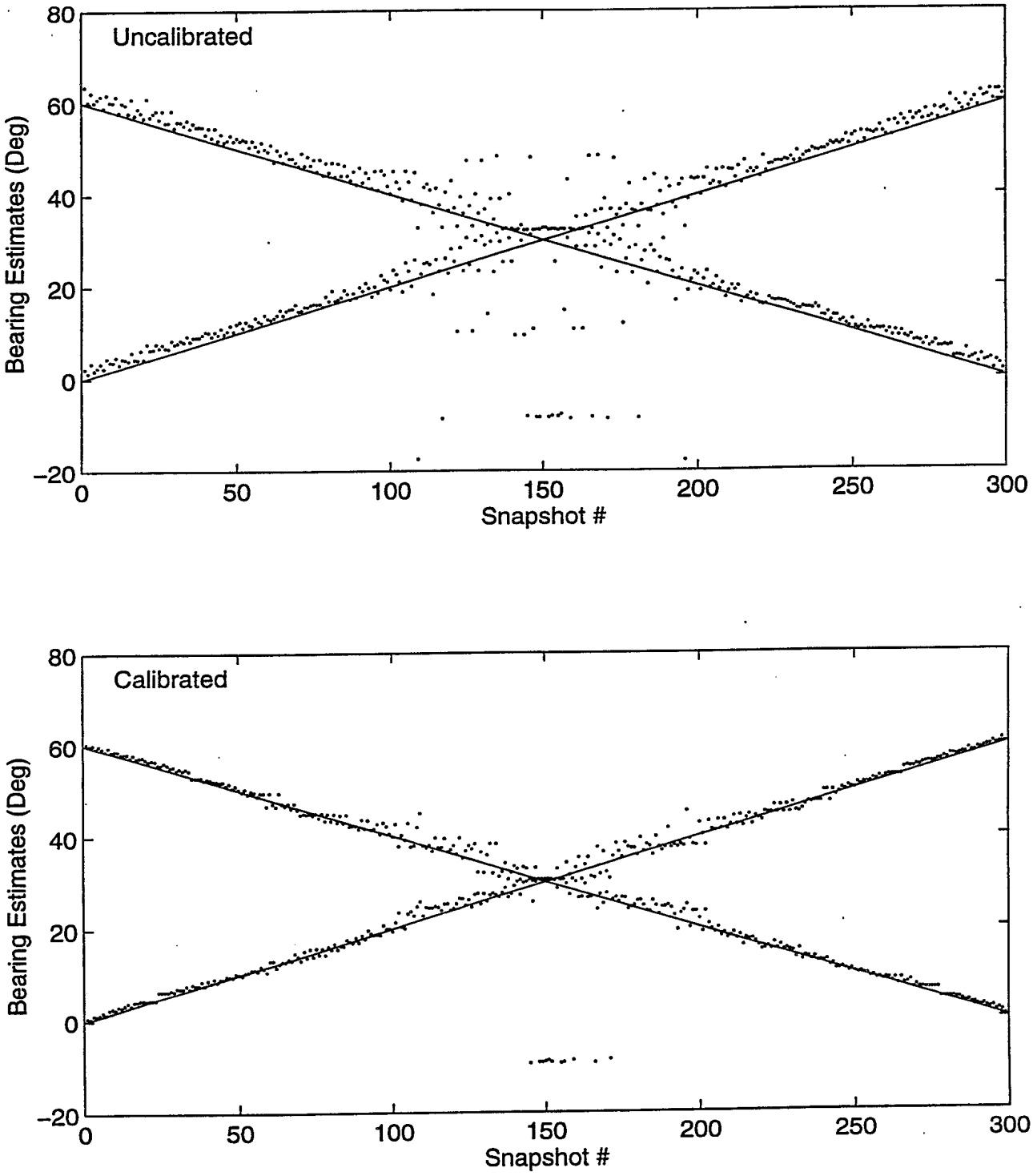

Figure 33. Bearing estimates (points) calculated with the data in File 3.

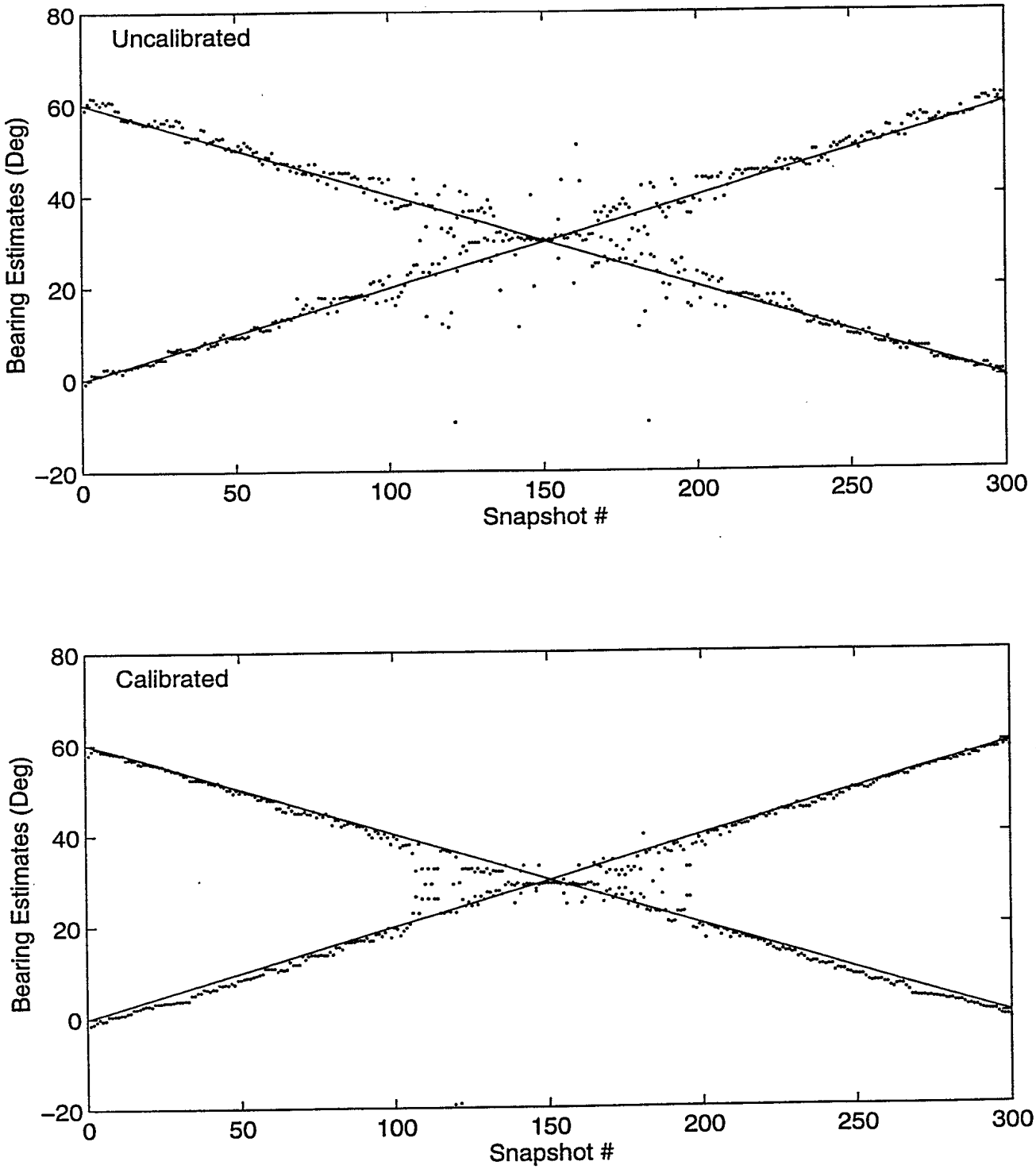

Figure 34. Bearing estimates (points) calculated with the data in File 4.

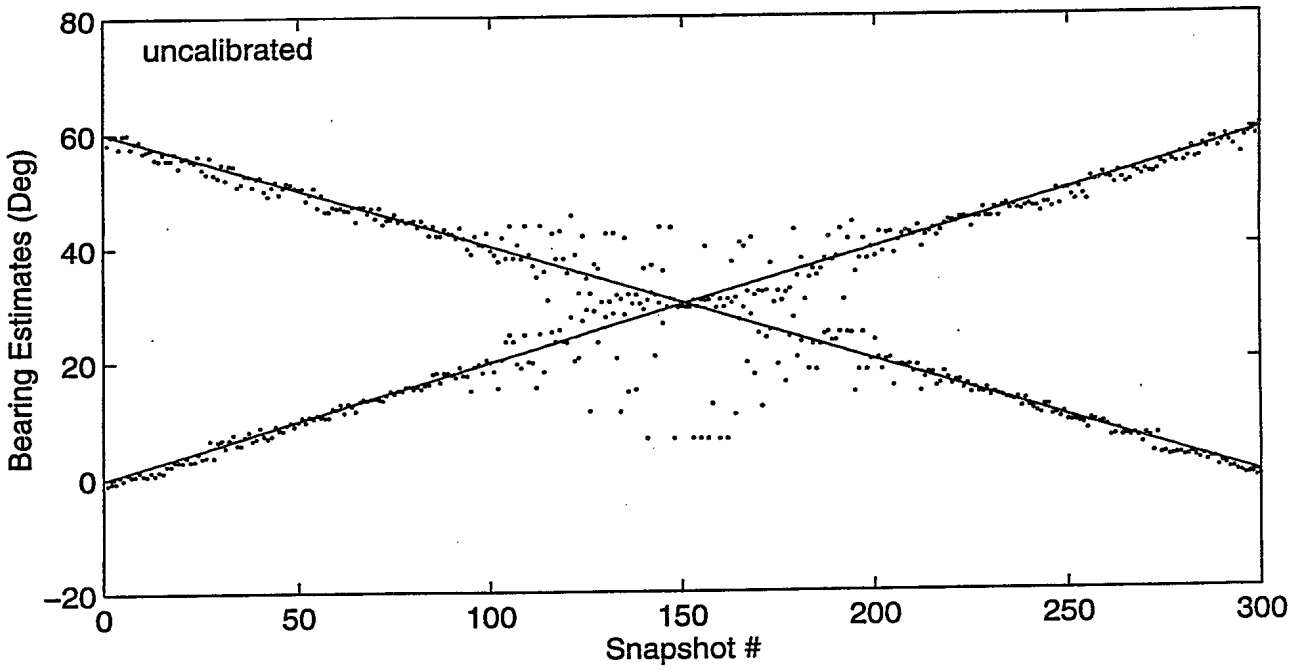

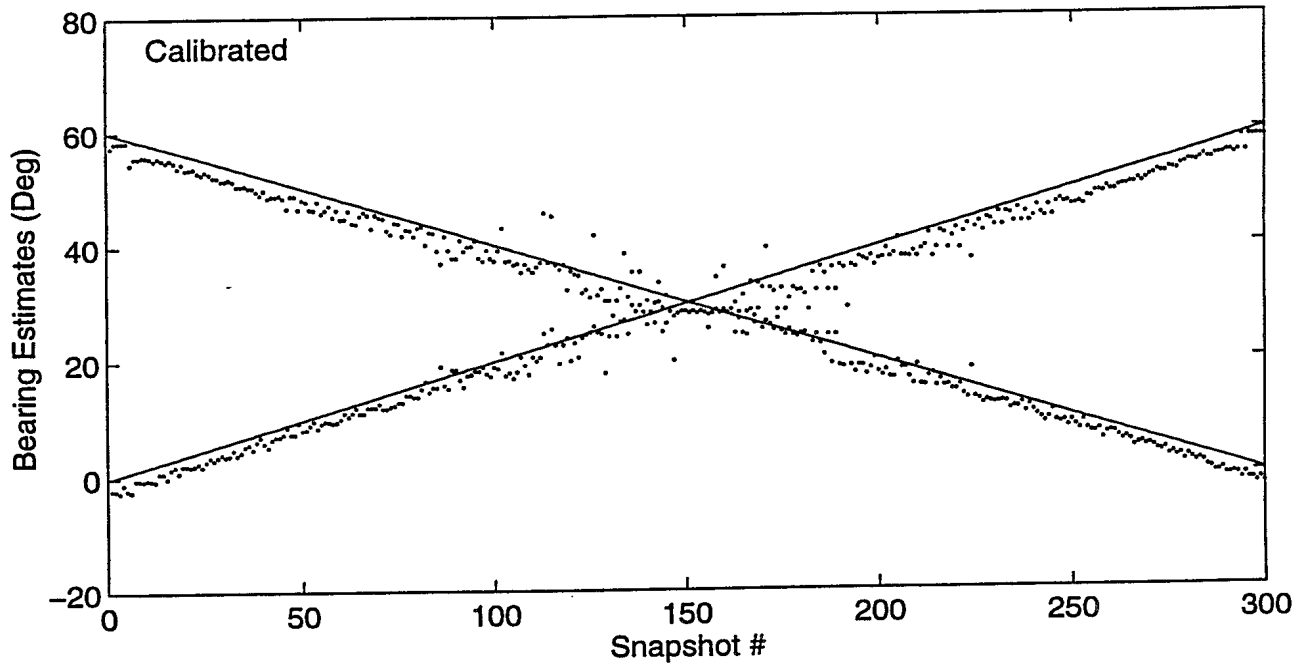

Figure 35. Bearing estimates (points) calculated with the data in File 5.

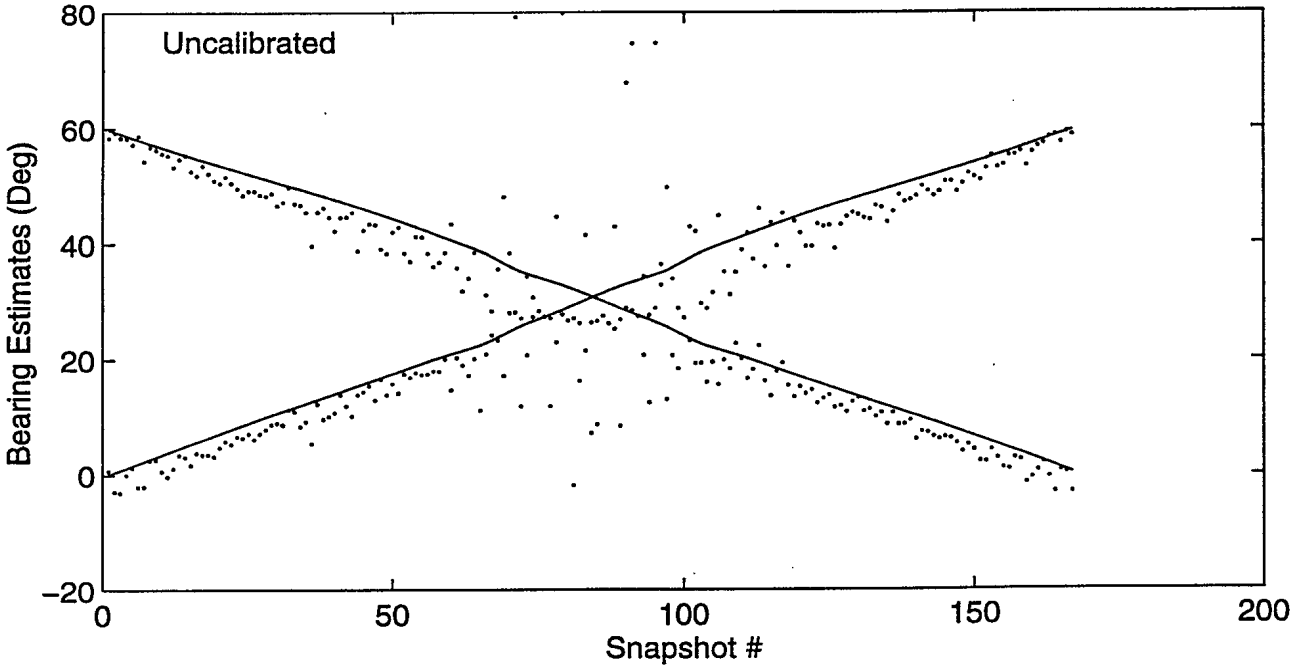

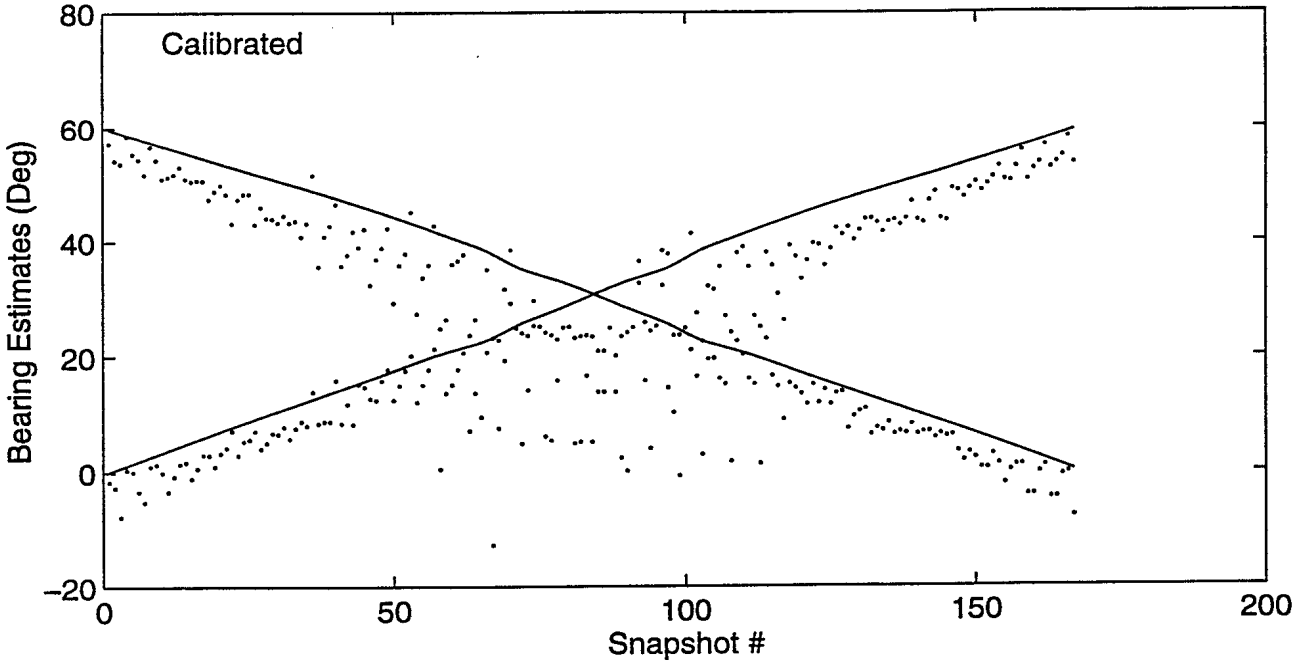

Figure 36. Bearing estimates (points) calculated with the data in File 6.

File	1	2	3	4	5	6
ψ(deg)	5.2	12.3	12.3	20.1	32.0	50.6
r(km)	10	7	7	5	3	2
J_B	25	25	28	25	27	18
J_A	10	11	12	23	18	24
PR (%)	60	56	57	8	33	-33

Table 7. Number of snapshots with unresolved signal directions, and the percentage reduction (PR) in the number of unresolved snapshots after calibration.

8.0 CONCLUSIONS

The authors have carried out an analysis of the 5.1 MHz calibration data measured with a high-frequency antenna array at Leitrim. The objective was to study whether the array calibration method developed by Hung in [8] is adequate for calibrating the HF antenna arrays in the CFSRS modernization project.

The following results were observed in the analysis of the data files generated with transmitter ranges not less than 7 km and transmitter elevations not higher than 11°.

1. With few exceptions, the calibration method increased the signal-to-interference-plus-noise ratio (SINR) in the array snapshots by a factor of 2 to 4 (3 to 6 dB).

2. The calibration method increased the accuracy of target direction estimates. More specifically, it reduced the standard deviation of the direction estimates by a factor of 3.0 or larger.

3. The method reduced the number of snapshots with unresolvable equal-strength targets in Files 1 to 5. The reduction is 56% or more for the first three files.

It is not possible to decide whether the method in [8] is adequate for calibrating the HF array antennas in the CFSRS modernization project. This decision requires a study of calibration data generated with transmitter ranges not less than 7 km and transmitter elevations higher than 11°. Data files with these characteristics are not available in this study.

The difficulties in using the higher elevation files prompted

the authors to study an alternative calibration method [11] that tolerates the dependence of calibration coefficients on directions. Preliminary results indicated that this alternative method was superior to the method in [8]. Because of these results, the authors have decided to stop further work on the method in [8] and direct the remaining efforts to the evaluation of the method in [11].

APPENDIX

JUSTIFICATIONS FOR USING DIRECTION ESTIMATES IN (7.2)

The true transmitter direction is not used in (7.2) to calculate $SINR_A$, $SINR_B$ and $SINR_C$. This direction cannot be determined precisely from the recorded GPS1 and GPS2 times. These times are not equal and there are uncertainties in the value of the time adjustment Δ' one should use in (3.2).

In a separate study, the following approaches to determine the transmitter direction were evaluated:

Method 1:

Identify the transmitter direction before calibration as the GPS direction calculated with (3.2) and $\Delta'=8.7$. Identify the direction after calibration as the GPS direction calculated with (3.2) and $\Delta'=7.4$.

Method 2:

Identify the transmitter direction before and after calibration as the GPS direction calculated with (3.2) and $\Delta'=8.7$.

Method 3:

Identify the transmitter direction before and after calibration as the GPS direction calculated with (3.2) and $\Delta'=7.4$.

Method 4:

Identify the transmitter direction before calibration as the direction estimated with the uncalibrated array snapshots. Identify the direction after calibration as the direction estimated with the calibrated array snapshots.

The decision to present only the results obtained with Method 4 are based on the following observations:

1. When the GPS direction is used, the values of $SINR_A$ and $SINR_B$ depend on Δ'. Using $\Delta'=7.4$ instead of $\Delta'=8.7$ could change these values by 1.0 dB or more.

   Remark: One can show that the dependence of $SINR_A$ and $SINR_B$ on Δ' originates from the dependence of the errors $\epsilon(\theta)$ and $\epsilon(\hat{\theta})$ on Δ'. A larger error results in a smaller value of the corresponding SINR.

2. With Method 4, the values of $SINR_A$ and $SINR_B$ do not depend on Δ'.

3. With Method 4, a positive value of $SINR_C$ corresponds to a higher probability of detecting the transmitter signal after calibration.

4. The values of $SINR_A$, $SINR_B$ and $SINR_C$ calculated with the Methods 1 to 3 are usually within 2 dB of those obtained with Method 4.

REFERENCES

1. R. O. Schmidt, "Multiple Emitter Location and Signal Parameter Estimation", IEEE Trans. Antennas and Propagation, vol. AP-34, pp. 276-280, March 1986.

2. A. Paulraj and T. Kailath, "Direction of Arrival Estimation by Eigenstructure Methods with Unknown Sensor Gain and Phase," ICASSP 1985, Tampa, U.S.A., pp.640-643, March 1985.

3. B. Friedlander and A. J. Weiss, "Eigenstructure Methods for Direction Finding with Sensor Gain and Phase Uncertainties," ICASSP 1988, New York, U.S.A., pp. 2681-2684, April 1988.

4. A. J. Weiss and B. Friedlander, "Eigenstructure Methods for Direction Finding with Sensor Gain and Phase Uncertainties," Circuits and Systems and Signal Processing, vol. 9, No. 3, pp.271-300, 1990.

5. G. C. Brown, J. H. McClellan and E. J. Holder, "A Phased Array Calibration Technique using Eigenstructure Methods," IEEE 1990 International Radar Conference, Arlington, U.S.A., pp.304-307, May 1990.

6. G. C. Brown, J. H. McClellan and E. J. Holder, "Eigenstructure Approach for Array Processing and Calibration with General Phase and Gain Perturbations," ICASSP 91, Toronto, Canada, pp.3037-3040, May 1991.

7. J. Pierre and M. Kaveh, "Experimental Performance of Calibration and Direction-Finding Algorithms," ICASSP 91, Toronto, Canada, pp.1365-1368, May 1991.

8. Eric Hung, "Calibration of an Array Antenna in the Presence of Multipath Interference," Symposium on Antenna Technology and Applied Electromagnetics, Winnipeg, Canada, pp.74-79, August 1992.

9. R.W. Jenkins, "Antenna Amplitude and Phase Pattern Measurements using an Aircraft-Towed Transmitter," CRC Report No. 95-003, Communications Research Centre, Ottawa, Ontario, September 1995.

10. J. Capon, "High-Resolution Frequency-Wavenumber Spectrum Analysis," Proceedings of the IEEE, vol. 57, pp. 1408-1418, August 1969.

11. Eric K.L. Hung, "Computation of the Coupling Matrix Among the Elements of an Array Antenna," 1994 International Conference on Radar, pp. 703-706, Paris, May 1994.

DOCUMENT CONTROL DATA

(Security classification of title, body of abstract and indexing annotation must be entered when the overall document is classified)

1. ORIGINATOR (the name and address of the organization preparing the document. Organizations for whom the document was prepared, e.g. Establishment sponsoring a contractor's report, or tasking agency, are entered in section 8.)

Department of National Defence
Defence Research Establishment Ottawa
Ottawa, Ontario, Canada K1A 0Z4

2. SECURITY CLASSIFICATION (overall security classification of the document. including special warning terms if applicable)

UNCLASSIFIED

3. TITLE (the complete document title as indicated on the title page. Its classification should be indicated by the appropriate abbreviation (S,C,R or U) in parentheses after the title.)

Analysis of the calibration data measured with a high-frequency antenna array near Ottawa (U)

4. AUTHORS (Last name, first name, middle initial)

Xinping Huang (Applied Silicon Inc. Canada)
Eric K.L. Hung (DREO/SR)

5. DATE OF PUBLICATION (month and year of publication of document)

6a. NO. OF PAGES (total containing information. Include Annexes, Appendices, etc.)

91

6b. NO. OF REFS (total cited in document)

11

7. DESCRIPTIVE NOTES (the category of the document, e.g. technical report, technical note or memorandum. If appropriate, enter the type of report, e.g. interim, progress, summary, annual or final. Give the inclusive dates when a specific reporting period is covered.)

Technical Report

8. SPONSORING ACTIVITY (the name of the department project office or laboratory sponsoring the research and development. Include the address.)

Department of National Defence
Defence Research Establishment Ottawa
Ottawa, Ontario, Canada K1A 0Z4

9a. PROJECT OR GRANT NO. (if appropriate, the applicable research and development project or grant number under which the document was written. Please specify whether project or grant)

05B09

9b. CONTRACT NO. (if appropriate, the applicable number under which the document was written)

W7714-4-0188

10a. ORIGINATOR'S DOCUMENT NUMBER (the official document number by which the document is identified by the originating activity. This number must be unique to this document.)

DREO REPORT 1289

10b. OTHER DOCUMENT NOS. (Any other numbers which may be assigned this document either by the originator or by the sponsor)

11. DOCUMENT AVAILABILITY (any limitations on further dissemination of the document, other than those imposed by security classification)

(X) Unlimited distribution
( ) Distribution limited to defence departments and defence contractors; further distribution only as approved
( ) Distribution limited to defence departments and Canadian defence contractors; further distribution only as approved
( ) Distribution limited to government departments and agencies; further distribution only as approved
( ) Distribution limited to defence departments; further distribution only as approved
( ) Other (please specify):

12. DOCUMENT ANNOUNCEMENT (any limitation to the bibliographic announcement of this document. This will normally correspond to the Document Availabilty (11). However, where further distribution (beyond the audience specified in 11) is possible, a wider announcement audience may be selected.)

UNCLASSIFIED

SECURITY CLASSIFICATION OF FORM

13. ABSTRACT (a brief and factual summary of the document. It may also appear elsewhere in the body of the document itself. It is highly desirable that the abstract of classified documents be unclassified. Each paragraph of the abstract shall begin with an indication of the security classification of the information in the paragraph (unless the document itself is unclassified) represented as (S), (C), (R), or (U). It is not necessary to include here abstracts in both offical languages unless the text is bilingual).

This report contains an analysis of the antenna calibration data taken with a high frequency (HF) antenna array and a pilot source towed behind a small aircraft. The analysis used an array calibration method developed by E.K.L. Hung. The objective was to determine whether this method was adequate for calibrating the HF antenna arrays in the Canadian Forces Supplementary Radio (CFSRS) modernization project.

The study showed that the calibration method significantly improved the performance of the array in detecting low-elevation (11° or less) targets and estimating their directions. The degree of improvement decreased as the target elevation increased. At an elevation of 49°, it was marginal at best.

This study also uncovered the presence of systematic errors in the calibration data. These errors increased rapidly with the pilot source elevation.

It is not possible to decide whether or not the calibration method is adequate for the CFSRS antenna arrays. In this study, the calibration method could be inadequate for high-elevation targets, or the method was adequate but the systematic errors negated the improvements gained in the calibration.

14. KEYWORDS, DESCRIPTORS or IDENTIFIERS (technically meaningful terms or short phrases that characterize a document and could be helpful in cataloguing the document. They should be selected so that no security classification is required. Identifiers, such as equipment model designation, trade name, military project code name, geographic location may also be included. If possible keywords should be selected from a published thesaurus. e.g. Thesaurus of Engineering and Scientific Terms (TEST) and that thesaurus-identified. If it is not possible to select indexing terms which are Unclassified, the classification of each should be indicated as with the title.)

Antenna Array
Calibration
High Frequency
Direction Finding

NO. OF COPIES NOMBRE DE COPIES	COPY NO. COPIE Nº	INFORMATION SCIENTIST'S INITIALS INITIALES DE L'AGENT D'INFORMATION SCIENTIFIQUE
1	1	BA
AQUISITION ROUTE ▶ FOURNI PAR		DREO
DATE ▶		17 Oct 96
DSIS ACCESSION NO. ▶ NUMÉRO DSIS		

DND 1158 (6-87)

National Defence / Défense nationale

499676

PLEASE RETURN THIS DOCUMENT TO THE FOLLOWING ADDRESS:

DIRECTOR
SCIENTIFIC INFORMATION SERVICES
NATIONAL DEFENCE
HEADQUARTERS
OTTAWA, ONT. - CANADA K1A 0K2

PRIÈRE DE RETOURNER CE DOCUMENT À L'ADRESSE SUIVANTE:

DIRECTEUR
SERVICES D'INFORMATION SCIENTIFIQUES
QUARTIER GÉNÉRAL
DE LA DÉFENSE NATIONALE
OTTAWA, ONT. - CANADA K1A 0K2